Blooms of the toxic dinoflagellate *Alexandrium fundyense* in the western Gulf of Maine in 1993 and 1994: A comparative modeling study

Charles A. Stock[a],*, Dennis J. McGillicuddy Jr[b], Donald M. Anderson[c], Andrew R. Solow[d], Richard P. Signell[e]

[a]*Woods Hole Oceanographic Institution, Woods Hole, MA 02540, USA*
[b]*Woods Hole Oceanographic Institution, Mail Stop 11, Woods Hole, MA 02543, USA*
[c]*Woods Hole Oceanographic Institution, Mail Stop 32, Woods Hole, MA 02543, USA*
[d]*Woods Hole Oceanographic Institution, Mail Stop 41, Woods Hole, MA 02543, USA*
[e]*United States Geological Survey, 384 Woods Hole Road, Woods Hole, MA 02543, USA*

Abstract

Blooms of the toxic dinoflagellate *Alexandrium fundyense* commonly occur in the western Gulf of Maine but the amount of toxin observed in coastal shellfish is highly variable. In this study, a coupled physical–biological model is used to investigate the dynamics underlying the observed *A. fundyense* abundance and shellfish toxicity in 1993 (a high toxicity year) and 1994 (low toxicity year). The physical model simulates the spring circulation, while the biological model estimates the germination and population dynamics of *A. fundyense* based on laboratory and field data. The model captures the large-scale aspects of the initiation and development of *A. fundyense* blooms during both years, but small-scale patchiness and the dynamics of bloom termination remain problematic. In both cases, the germination of resting cysts accounts for the magnitude of *A. fundyense* populations early in the spring. Simulations with low net *A. fundyense* growth rates capture the mean observed concentration during the bloom peak, which is of similar magnitude during both years. There is little evidence that large-scale changes in biological dynamics between 1993 and 1994 were a primary driver of the differences in shellfish toxicity. Results instead suggest that the persistent southwesterly flow of the western Maine Coastal Current led to *A. fundyense* populations of similar alongshore extent by late May of both years. This period coincides with peak cell abundance in the region. Variations in wind forcing (downwelling favorable in 1993, upwelling favorable in 1994) and subsequent cell transport (inshore in 1993, offshore in 1994) in early June then provides a plausible explanation for the dramatic mid-June differences in shellfish toxicity throughout the western Gulf of Maine.
© 2007 Elsevier Ltd. All rights reserved.

Keywords: Red tides; Algal blooms; Harmful algal blooms; Modeling; Paralytic shellfish poisoning

*Corresponding author. Present address: NOAA/Geophysical Fluid Dynamics Laboratory, Princeton University Forrestal Campus, 201 Forrestal Road, Princeton, NJ 08540, USA. Tel.: +1 609 452 6500x6971; fax: +1 609 987 5063.

E-mail addresses: cstock@alum.mit.edu (C.A. Stock), dmcgillicuddy@whoi.edu (D.J. McGillicuddy Jr), danderson@whoi.edu (D.M. Anderson), asolow@whoi.edu (A.R. Solow), rsignell@usgs.gov (R.P. Signell).

1. Introduction

Blooms of the toxic dinoflagellate *Alexandrium fundyense* have occurred within the coastal waters of the western Gulf of Maine (WGOM) since at least 1972 (Shumway et al., 1988; Anderson, 1997). The toxins produced by this organism lead to paralytic shellfish poisoning (PSP), a potentially fatal malady associated with the consumption of shellfish exposed to *A. fundyense*. While toxins are frequently detected in the region's shellfish and closures of shellfish beds occur nearly every year, the spatial and temporal patterns of cell abundance and shellfish toxicity are variable (e.g., Franks and Anderson, 1992b; Anderson et al., 2005a, b; Luerssen et al., 2005; McGillicuddy et al., 2005). In this study, a coupled physical–biological model is used to investigate the dynamics underlying observed differences in shellfish toxicity and cell abundance in 1993 (a high toxicity year) and 1994 (a low toxicity year).

A strong connection between *A. fundyense* bloom patterns in the Gulf of Maine and regional circulation is supported by numerous studies (Franks and Anderson, 1992a, b; Anderson et al., 2005a; Keafer et al., 2005; Luerssen et al., 2005). During the spring and summer in the Gulf of Maine, a southwestward flowing coastal current is

driven by density gradients between fresh water near the coast and denser, more saline water offshore and within the Gulf's three deep basins (Fig. 1, Bigelow, 1927; Brooks, 1985). This flow is divided into a series of segments and branch points (Lynch et al., 1997). The segment to the north and east of Penobscot Bay is referred to herein as the eastern Maine Coastal Current (EMCC), and that to the south and west as the western Maine Coastal Current (WMCC).

Franks and Anderson (1992b) observed that the spring onset of shellfish toxicity in the WGOM often shows a northeast to southwest progression that is consistent with the WMCC-driven transport of *A. fundyense* populations originating near Casco Bay or further north. Many cells were observed within the plume of the Kennebec and Androscoggin (K/A) rivers. This, along with the observation that the southwestern extent of shellfish toxicity was positively correlated with May K/A river inputs, suggested that the magnitude of the K/A river outflow may play a key role in determining the extent of *A. fundyense* alongshore transport. It was further observed that upwelling-favorable winds (i.e. toward the east or northeast) moved the plume and associated cells offshore, while downwelling winds (toward the west or southwest) delivered the plume and cells to the coast, favored toxicity in
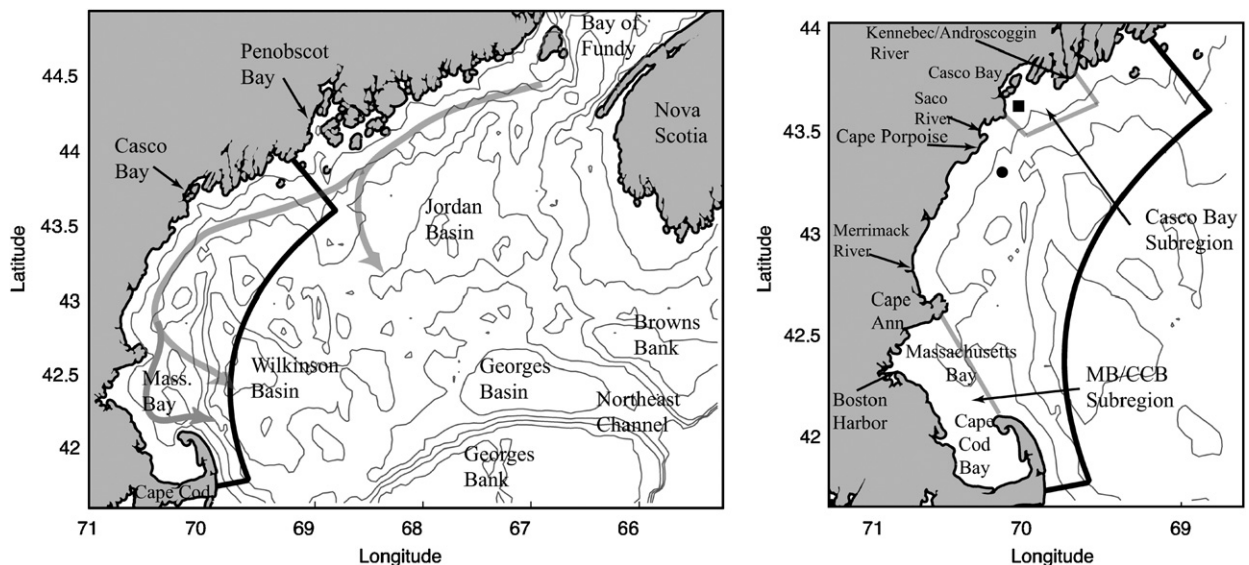
Fig. 1. Left panel: The Gulf of Maine and study region. The study domain is outlined in black. Depth contours are at 50, 100, 150, and 200 m. The direction of flow of the Maine Coastal Current (adapted from Lynch et al., 1997) is shown as a thick gray line. Branch points offshore of Penobscot Bay and Cape Ann are notable. Right panel: close-up of study region. The solid circle is the location of the Cape Porpoise current meter, the solid square is the location of the Portland Meteorological Buoy.

coastal shellfish beds, and increased southwest transport. These elements were combined to form the "plume advection hypothesis" for the factors governing *A. fundyense* bloom dynamics and shellfish toxicity in the WGOM (Franks and Anderson, 1992a, b).
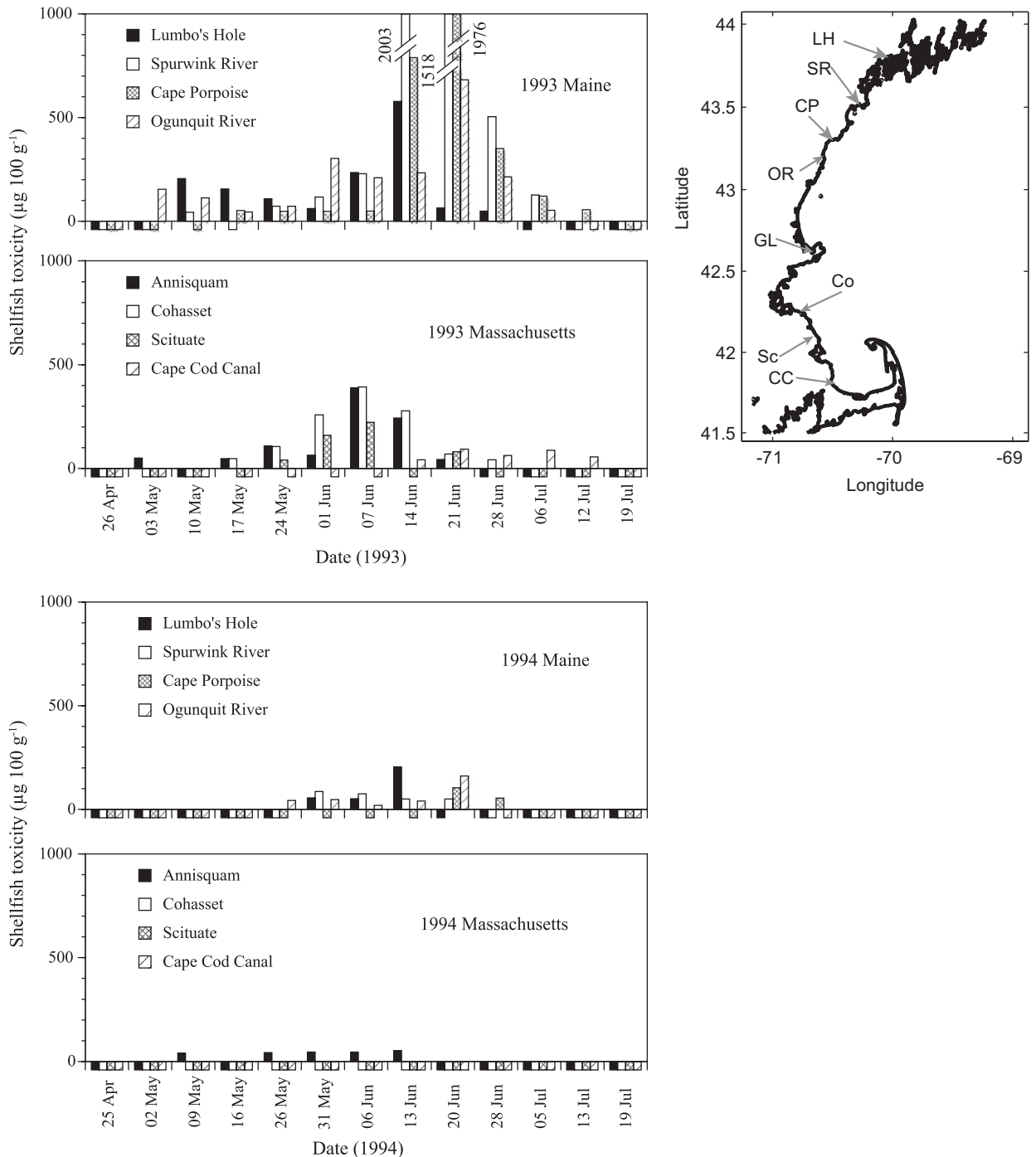
Fig. 2. Weekly time series of shellfish toxicity (μg of saxitoxin equivalents per 100 g of shellfish meat) in the blue mussel *Mytilus edulis* reported for key stations in Maine and Massachusetts during the 1993 and 1994 *A. fundyense* bloom seasons (Anderson et al., 2005a, toxicity panel Copyright (2005) by the American Society of Limnology and Oceanography, Inc., reprinted with permission). Locations of the shellfish monitoring stations are noted with closed circles and 2 letter codes. Codes are as follows: LH, Lumbo's Hole; SR, Spurwink River; CP, Cape Porpoise; OR, Ogunquit River; Gl, Gloucester-Annissquam; Co, Cohasset; Sc, Scituate; CC, Cape Cod Canal.

The elements of this hypothesis were tested using extensive physical and biological data collected during the springs of 1993 and 1994 (Geyer et al., 2004; Anderson et al., 2005a). In 1993, shellfish toxicity was very high throughout the WGOM, including Casco Bay, Massachusetts Bay, and Cape Cod Bay (MB/CCB, Fig. 2). In 1994, shellfish toxicity was low and restricted to areas north of Cape Ann. Interestingly, K/A river outflow in May of 1994 was larger than that observed in 1993 (Fig. 3, top panel). In addition, detailed analysis of the WMCC in 1994 suggests that less than half of the near surface flow velocity was derived from baroclinic gradients associated with river plumes generated by the K/A and Penobscot rivers (Geyer et al., 2004). This suggests decreased importance of local river inputs for the alongshore propagation of *A. fundyense* and led Anderson et al. (2005a) to suggest that predominant upwelling wind conditions (Fig. 3, bottom panel) from late March to mid-May in 1994 were likely responsible for the delayed timing, reduced alongshore extent, and reduced severity of shellfish toxicity in 1994.

Herein, we use a coupled physical–biological to evaluate the extent to which existing conceptual models can explain observed patterns in cell abundance. First, uncertain biological model parameters are tuned to fit the data during each year. This reveals (1) the degree to which the model can match observed patterns, (2) the degree to which uncertain model parameters can be constrained by the observations, and (3) if there is evidence for a large shift in biological dynamics between the 2 years. Simulations are then diagnosed to understand the properties of those simulations that match observed bloom patterns and the dynamics underlying remaining model-data misfits. In particular, the impact of large-scale variations in factors influencing rates of germination and growth (e.g., temperature, nutrients, light) on large-scale patterns in cell abundance and shellfish toxicity is assessed. The primarily physical explanations of shellfish toxicity variability offered by Franks and Anderson (Franks and Anderson, 1992a, b) and Anderson et al. (2005a) are then revisited.

2. Methods

2.1. Observations

The observations used here were collected during a Regional Marine Research Program study (hereafter "RMRP surveys"). Survey data are summarized in Table 1, with detailed descriptions found in Anderson et al. (2005a), Geyer et al. (2004), and Martorano and Loder (1997). *A. fundyense* cell counts were taken at the surface and, for a subset of the stations (~60%) at 10 m. Measurements at 10 m
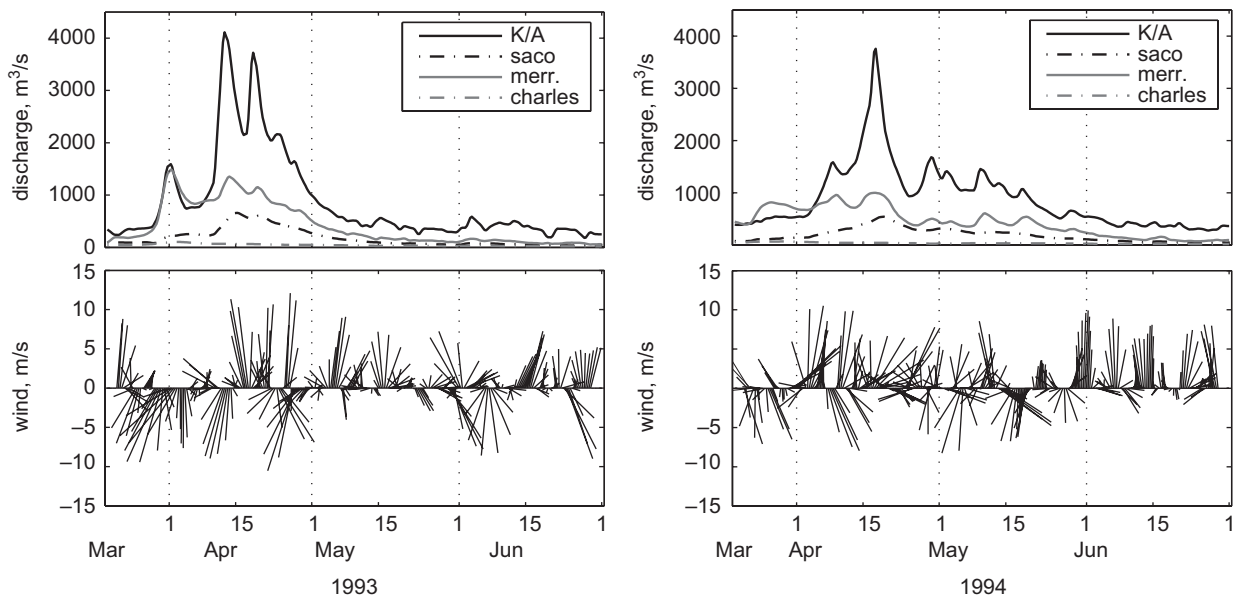
Fig. 3. The wind and river flows for 1993 (left column) and 1994 (right column). In the top panels are the discharges for the Kennebec/Adroscoggin (K/A), Saco, Merrimack, and Charles rivers. The bottom panels give stick plots of the observed winds at the Portland meteorological buoy. Wind data have been filtered with a 2-day low-pass filter.

Table 1
Summary of RMRP survey activities

Year-Cruise	Dates	# Stations	Coverage	DIN
1993-1	4/12–4/14	64	Full	y
1993-2	4/28–4/30	80	Full	y
1993-3	5/10–5/13	84	Full	y
1993-4	5/24–5/27	87	Full	y
1993-5	6/4–6/6	88	Full	y
1994-1a	4/28–5/1	105	Full	y
1994-1b	5/2–5/4	110	Full	y
1994-2	5/10–5/11	31	Casco Bay region to Cape Porpoise	n
1994-3	5/21	9	Cape Porpoise	n
1994-4	5/24–5/25	24	Cape Porpoise, Cape Ann, Boston Harbor	y
1994-5a	6/1–6/3	111	Full	y
1994-5b	6/4–6/5	59	Casco Bay to Merrimack River	n
1994-6	6/10–6/11	44	Casco Bay to Cape Porpoise	y
1994-7	6/15–6/17	27	Cape Cod Bay	y
1994-8	7/1	10	Cape Porpoise	n

All cruises included sampling of hydrography and *A. fundyense* concentrations. A total of 386 stations had successful surface sampling of *A. fundyense* in 1993, and a total of 515 stations successfully sampled surface *A. fundyense* in 1994. "Full" coverage refers to relatively complete coverage of the coastal region within the model domain. The "DIN" column specifies whether nutrient data was collected on the cruise. Plots of data from many of these cruises will be included within the model/data comparison in Section 3.

were correlated with surface measurements, particularly over the larger scales of interest in this study (after log transform, the correlation coefficient is 0.63 point-to-point basis, 0.88 based on cruise-by-cruise averages). The more numerous surface measurements are thus used as the basis for the model-data comparison. Hydrographic and nutrient data including phosphate, silicate, nitrate, nitrite, and ammonium were also collected. Nitrogen was generally limiting assuming Redfield stoichiometry (Martorano and Loder, 1997). Moorings were deployed (Geyer et al., 2004), and the Cape Porpoise P2 location (Fig. 1) common to both years is used herein. Currents were measured at 5, 27, and 50 m.

Survey coverage and timing during the 2 years is notably different, reflecting a change in sampling strategy. In 1993, 5 cruises of roughly equal temporal spacing (~2 weeks) provided coverage of the majority of the domain. The 1994 surveys sought to examine short-term changes in the cell distribution by conducting repeated large-scale surveys with a separation of only several days. The large-scale surveys were augmented by ancillary cruises with partial study area coverage. The 1994 surveys also started later in the season (April 28 versus April 12), but continued through June. These changes required adjustments to the methodology of Stock et al. (2005), most notably a change in the

manner by which the concentration of dissolved inorganic nitrogen (DIN) is specified (see below).

2.2. Physical model

The physical component of the model is provided by the 3D, non-linear Estuarine, Coastal and Ocean Model (ECOM) (Blumberg and Mellor, 1987; see Table 2, Fig. 3 for model forcing). Most elements of the physical simulation are detailed in Stock et al. (2005). However, several notable adjustments were made. First, the horizontally uniform initial salinity profiles were adjusted to reflect more salty conditions in the top 50 m prior to the spring freshet in 1994 (~32.6–32.8 ppt) than in 1993 (~32.1–32.3 ppt). Values were set based on moored measurements from mid to late March at the Cape Porpoise mooring (Fig. 1, Geyer et al., 2004). The salinity at depths >150 m is based on climatology (Naimie et al., 1994), with values between 50 and 150 m used to blend the observations and climatology (Table 2).

Second, the simulation was lengthened to include all of the 1994 data and now ends on July 1 rather than June 6. To maintain simulation stability over the longer simulation time, the barotropic boundary condition was switched from a combination of clamped and radiation conditions to a Flather condition (Flather, 1976). This allows locally

Table 2
The physical model forcing

Forcing	Source/description
Wind	Portland off-shore buoy (NDBC #44007), applied throughout domain and translated to shear via Large and Pond (Large and Pond, 1981). A 6% increase in wind speed relative to Stock et al. (2005) was applied to properly account for instrument height. The influence of this correction on model dynamics was negligible
Boundary depth-averaged currents and sea surface elevation	M_2 tidal depth averaged velocity and sea surface elevation from Gulf of Maine tidal model (Lynch and Naimie, 1993). Residual depth averaged velocity and sea surface elevations from bi-monthly climatology (Naimie et al., 1994; Lynch et al., 1997). Modified using ADCIRC-based barotropic wind response (see text and online supporting material for this paper).
River discharge	USGS stream gauges at 4 major rivers: Charles, Saco, Merrimack, and the Kennebec/Androscoggin
Boundary T,S	Interpolated and extrapolated from mooring and survey data ($>150\,\mathrm{m}$), climatology at depth (Naimie et al., 1994).
Initial T,S	Horizontally uniform initial T, S profiles. Top $50\,\mathrm{m}$ based on moored measurements at 5 and $50\,\mathrm{m}$ (1993) and 5, 27, and $50\,\mathrm{m}$ (1994) during mid to late March at the Cape Porpoise mooring (Fig. 1; see Geyer et al., 2004 for details). T and S for depths $>150\,\mathrm{m}$ are based on climatology (Naimie et al., 1994), and values between 50–$150\,\mathrm{m}$ blend the observations and climatology.
Heat flux	Shortwave radiative heat flux from land-based sensor at Woods Hole Sensible and latent heat fluxes estimated using Portland off-shore buoy data and the bulk formulae of Large and Pond (1982). Longwave flux estimated using Portland off-shore buoy data and relationships of Berliand and Berliand as described in Fung et al. (1984). Model sea surface temperature also nudged toward observed fields using observed fields constructed from CTD casts and 8 day best AVHRR Oceans Pathfinder sea surface temperatures (see Stock et al., 2005)

generated dynamics that depart from climatological expectations at the boundary to propagate outward at the gravity wave speed. Additional meteorological and river data were readily available for longer simulation time (i.e., Fig. 3). However, boundary conditions for temperature and salinity in late June were simply held at conditions during the last period when substantial data were available (June 6 in 1993, June 10 in 1994). In addition, the temperature and salinity boundaries for the first cruise of 1994 (April 28), which show considerable freshening along the northern boundary due to the outflow of the Penobscot river (Fig. 1), were applied on April 15 so that this freshening coincided with the Penobscot River's spring freshet.

Lastly, a more complete wind response was implemented along the boundary. Previous efforts using this model domain (e.g., Stock et al., 2005) included direct coupling of wind stress and water velocity at the boundaries through drag on the ocean surface. However, clamping the sea surface to climatological values prevented any wind-driven set-up or set-down of the sea surface at the boundary sea surface (and associated barotropic currents). An approximation of this response was derived from a series of wind-driven

simulations using the depth-integrated Advanced Circulation Model for Coasts, Shelves and Estuaries (ADCIRC-2DDI, Luettich et al., 1992). Details of this function can be found in the online supporting material for this paper.

2.3. The biological model

The baseline biological model contains parameterizations of the germination and growth[1] of *A. fundyense* and is summarized in Fig. 4 and Table 3. More detailed descriptions of the functions and rationale can be found in Stock et al. (2005) and Anderson et al. (2005c). The model has only one biological state variable: the concentration of *A. fundyense* vegetative cells. This is justified on the basis that *A. fundyense* generally constitutes a small fraction of the total phytoplankton biomass. The influence of the broader ecosystem on *A. fundyense* abundance is therefore represented through its

---

[1]Note that "growth" in this manuscript is used solely to refer to changes in abundance driven by cell division rather than changes in the size of individual cells. Net growth is used to refer to changes in cell abundance resulting from growth minus losses of cells via mortality.
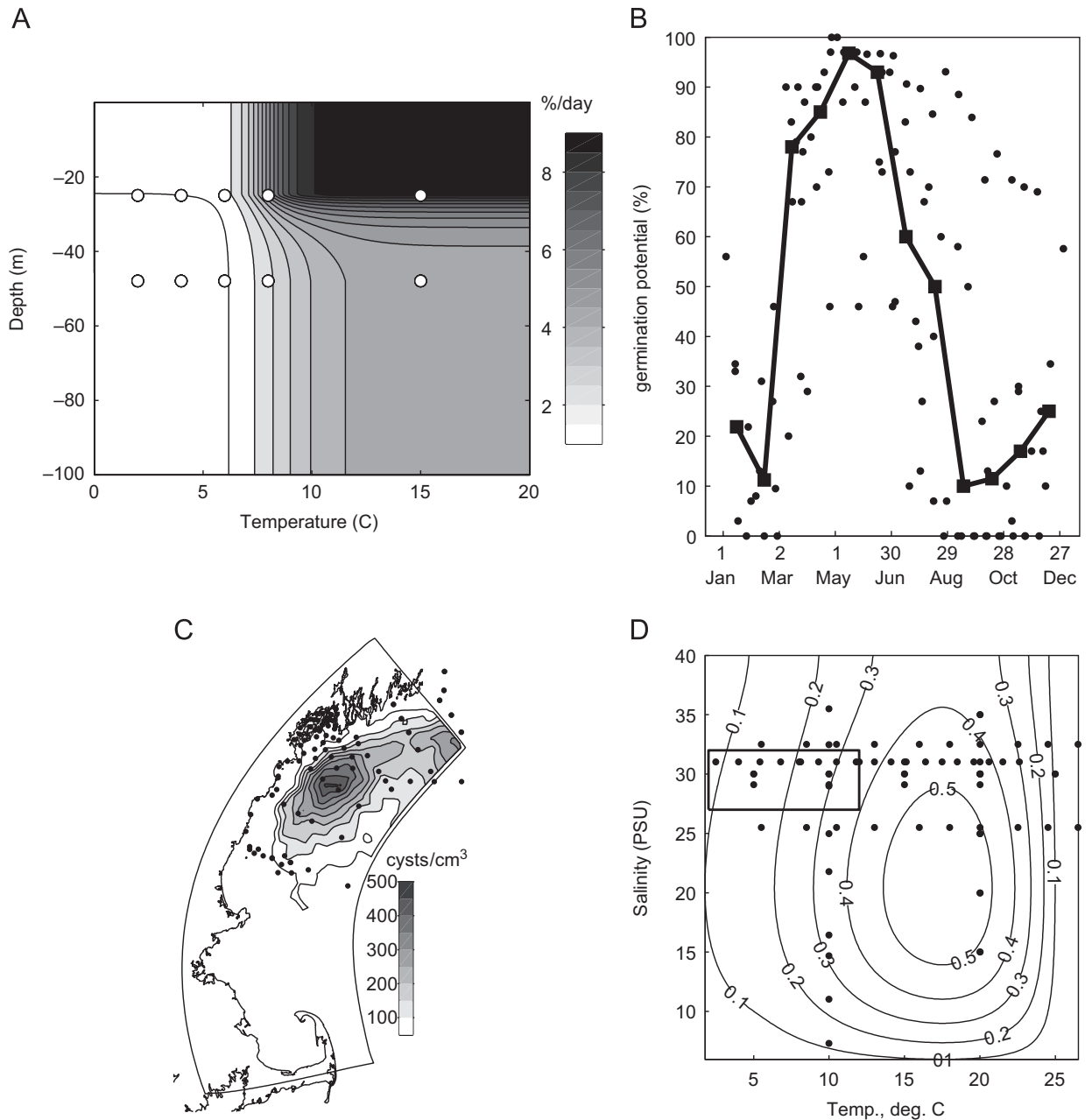
Fig. 4. (A)–(D). The baseline biological model summary (Stock et al., 2005, panels reprinted with permission from Elsevier). Observations are marked by dots on all plots. The germination rate is estimated as a function of temperature and light experienced by the resting cyst according to the laboratory-derived relationship (A) (note that light has been translated to depth in the water column using a diffuse irradiance attenuation of $0.2\,m^{-1}$, which is typical for coastal Gulf of Maine waters). This rate is modified according to the germination potential (B), which is controlled by an internal endogenous clock. The resulting rate is applied to a mapping of benthic cysts (C) to provide an estimate of the germination source. Once germinated, the cells swim up in the water column and grow according to the rates in panel (D) and a hyperbolic light/growth curve of the form suggested by Platt and Jassby (1976) for photosynthesis (not shown). Nutrient limitation and mortality are added to this baseline model and influence the growth rate as described in Section 2.3.

impact on the vital rates within the *A. fundyense* population dynamics model. Sensitivity analysis (Stock et al., 2005) shows that two parameters are

the dominant sources of uncertainty in the baseline model: the maximum growth rate μ_{max} and the germination depth d_g (see Table 3).

Table 3
Summary of biological model parameters and ranges

Symbol	Definition	Units	Range	Sources
K_N	Half-saturation constant for nutrient limited growth	μM	0–3	Eppley et al. (1969), Eppley and Thomas (1969), Lomas and Glibert (2000), Carpenter and Guillard (1971), MacIsaac et al. (1979), Sommer (1991)
m	Spatially and temporally averaged mortality rate	day^{-1}	0–0.3	See text
$\mu_{max}(T_{opt}, S_{opt})$	The maximum growth rate under optimal temperature and salinity conditions	day^{-1}	0.46–0.70	Cullen (unpublished data), Langdon (1987), Etheridge et al. (2005), Watras et al. (1982), Keafer and Kulis (unpublished data)[a]
μ_o^r	The maintenance respiration rate	day^{-1}	0.15–0.25	Cullen (unpublished data)
α_g	The growth efficiency	$day^{-1} W^{-1} m^2$	0.017–0.056	Cullen (unpublished data)
d_g	The mean depth of sediment over which cysts are able to germinate and contribute to the bloom	cm	0.5–1.5	Anderson et al. (2005c)
E_{lgt}	Light level for germination under "light" conditions	watts/m^2	1.2–3.6	Anderson et al. (2005c)
E_{drk}	Light level for germination under dark conditions	watts/m^2	0.1% of E_{lgt} to 10% of E_{lgt}.	Anderson et al. (2005c)
k_w	Mean diffuse attenuation in water column	m^{-1}	0.15–0.25	Townsend et al. (2001)
k_s	Mean diffuse attenuation in the sediment	mm^{-1}	2–5	Kuhl and Jorgensen (1994)
w_a	Vertical swimming speed	m/day	5–15	Bauerfeind et al. (1986), Kamykowski et al. (1992)

[a]Sources used for formulation of the growth versus temperature dependence polynomial are: Etheridge and Roesler (2005), Langdon (1987), Watras et al. (1982), and Keafer and Kulis (unpublished data). Sources used for the salinity dependence polynomial are: Etheridge and Roesler (2005) and Prakash (1967).

Two additional factors potentially limiting *A. fundyense* net growth are also considered: mortality and nitrogen-dependent growth. Mortality m is defined as a vegetative cell being removed from the water column. It is meant to represent the mean loss rate of *A. fundyense* via cell mortality, zooplankton grazing, and encystment over the course of the bloom and is applied as a constant average rate (day^{-1}). The intent of applying mortality in such a rudimentary way is to evaluate the necessity of a first order loss term to recreate the observed bloom magnitude, given knowledge of the *A. fundyense* germination and growth dynamics.

Dependence of population growth on DIN is modeled by the Monod formulation with half-saturation K_N. This formulation cannot capture the possible decoupling of nutrient uptake and growth over short time scales (e.g., Droop, 1983), but is suitable for assessing dependence of the population growth rate on ambient nutrients over seasonal time scales and remains in common use

(e.g., Denman and Pena, 1999; Chai et al., 2002; Spitz et al., 2003).

DIN concentrations in the surface waters of the WGOM are estimated using a relationship between DIN and temperature and salinity constructed from RMRP surface nutrient data (Figs. 5(A)–(C)). This function is applied over the top 21 m, which corresponds to a mean depth of the compensation light intensity for *A. fundyense* with parameters set to central values in Table 3. Below this depth, light is presumed limiting via Liebig's law of the minimum (Liebig, 1845). Previous efforts (Stock et al., 2005) specified surface DIN based on a linear interpolation between observations during regularly spaced cruises covering the majority of the model domain. The less regular temporal intervals between the 1994 cruises, their more variable spatial coverage, and the fact that the first cruise in 1994 was taken after the spring bloom, makes this approach less practical. Relationships for nitrate and Gulf of Maine hydrography exist (Garside et al., 1996) but
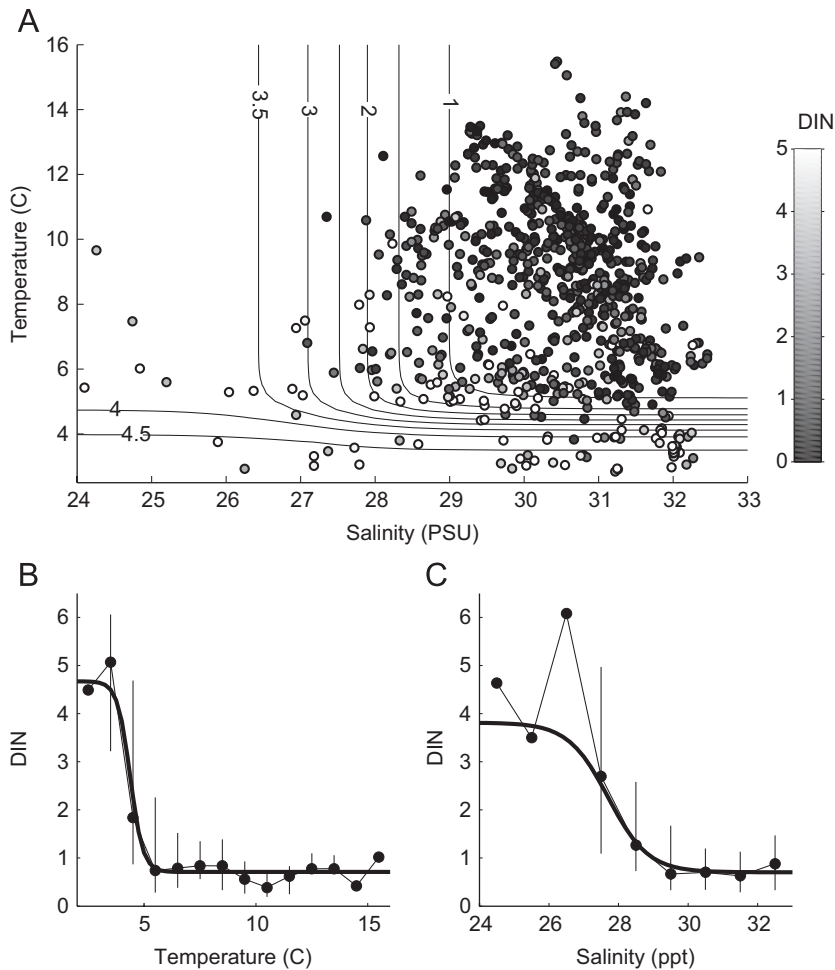
Fig. 5. (A) The functional relationship between surface temperature, salinity and DIN based on the 1993 and 1994 data sets. Contour interval = 0.5 μM. (B) Comparison of functional fit for DIN at 31.25 PSU (thick line) and the observed median DIN concentration in 1 °C bins for all data between 30 and 32.5 PSU (●). The vertical lines show the range of the middle two quartiles of the ordered set of observations about the median. Ranges are shown only for bins with >4 observations. (C) Comparison of the function fit for DIN in river water at 10 °C versus the median of all observations from 5 to 13 °C binned into 1 PSU intervals. Other markings are as in (B).

are not used here because the RMRP relationship yields a better fit for surface waters in the WGOM region in 1993 and 1994.

The functional fit based on RMRP data has a sharp decline of DIN between 2 and 5 °C (Figs. 5(A) and (B)), coinciding with typical surface water temperatures during the spring bloom in the Gulf of Maine (Townsend and Cammen, 1988). DIN is also elevated in fresher waters (Fig. 5(C)). The seasonal decline of DIN in surface waters during the spring is a primary feature of regional-scale nutrient variability in the surface waters of the WGOM (Petrie and Yeats, 2000). However, there is substantial small-scale variability apparent in the data

that is not captured by this function. Limitations imposed by this will be discussed, but capturing prominent seasonal trends provides a starting point for assessing the role of nutrients in shaping *A. fundyense* bloom dynamics.

A consistent outlier occurs at the station immediately adjacent to Boston Harbor, which tends to have elevated nitrogen regardless of temperature or salinity. This pattern is attributed to nutrient inputs from Boston and the robust nature of this result is supported by more detailed, concurrent studies of the region (Kelly and Doering, 1997). The DIN concentration at Boston Harbor was thus specified as the mean of the

observations taken during the 1993/1994 surveys (5.95 μM).

The equation governing the evolution of *A. fundyense* within the domain is

$$\frac{\partial C}{\partial t} + \nabla \cdot ((v + w_a)C) = \nabla \cdot K \nabla C + \mu C - mC + F_g,$$

where C is the concentration of *A. fundyense*, v the fluid velocity, w_a the vertical swimming rate of *A. fundyense*, K the diffusivity, μ the growth rate, m the mortality rate, and F_g is the change in concentration due to the flux of new cells from the sediment via germination. Swimming speed is attenuated in the euphotic zone so that general consistency with the surface to 10-m *A. fundyense* concentrations is maintained. The initial concentration of *A. fundyense* is set to 0 everywhere, as the beginning of the run (March 19) is generally before the start of the bloom season. Boundary concentrations are set to the mean concentration along the northernmost transect along the northern boundary and the first 25 km of the eastern boundary, and set to zero elsewhere. This differs slightly from the approach of Stock et al. (2005), which used an exact along-coast spatial extrapolation of individual observations to the northern boundary. It was found that water parcels passing the northern-most transect could originate from various points along the northern boundary depending on wind conditions and often traveled parallel to the curving bathymetry. The modified specification of the boundary condition thus proved more effective at matching observed cells at this transect.

2.4. The model/data comparison

The model is fit to data using the method of maximum likelihood, applied as described in detail by Stock et al. (2005). Briefly, misfits are assumed to be stochastic, and the best parameter estimates are obtained by maximizing the joint probability of all M misfits. The fit is optimized over the two dominant sources of uncertainty in the baseline model (μ_{max} and d_g) and the additional potential controls on net growth (K_N and m). Other parameters are given central values in their uncertainty ranges (Table 3). A lognormal distribution is assumed, and the likelihood L is written:

$$L(\mu_{max}, d_g, m, K_N; \varepsilon) = \frac{\exp(-(1/2)\varepsilon^T C_{\varepsilon\varepsilon}^{-1} \varepsilon)}{(2\pi)^{M/2}\sqrt{\det(C_{\varepsilon\varepsilon})}}.$$

Here "det" is the determinant, and ε is a vector of M misfits between the observed *A. fundyense* concentration (c_{obs} in cells/L) and that modeled (c_{mod}) at each observation point:

$$\varepsilon_i = \ln(c_{obs,i} + 1) - \ln(c_{mod,i} + 1).$$

$C_{\varepsilon\varepsilon}$ is a covariance matrix of the form (see Stock et al. (2005) for justification):

$$C_{ij} = \rho_{\Delta t}\sigma^2 \exp\left(-r_y\sqrt{\Delta y_{ij}^2 + \left(\frac{r_x}{r_y}\Delta x_{ij}\right)^2}\right),$$

where C_{ij} is the covariance between any two points i and j, σ^2 the estimated misfit variance and lies along the diagonal of the covariance matrix, Δx_{ij} and Δy_{ij} are the approximate cross-shore and along-shore distances between i and j (km), r_x and r_y are the cross-shore and along-shore covariance decay coefficients (km^{-1}), and $\rho_{\Delta t}$ is a temporal covariance term and is given the form:

$$\rho_{\Delta t} = \exp(-r_t \Delta t_{ij}),$$

where Δt_{ij} is the time between any two observations i and j (days separating the mid-points of each cruise, 0 if the observations were taken during the same cruise), and r_t is a temporal decay coefficient (days^{-1}). This last element differs slightly from the form of Stock et al. (2005), where equal cruise spacing in 1993 allowed a discrete representation temporal decorrelation. However, results are not sensitive to the differences between these two formulations.

Confidence intervals around the best parameter estimates are constructed using a maximum likelihood ratio test. Analysis focuses on determining the degree to which biological model parameters, in particular K_N and m, can be constrained by the data and evaluating evidence for parameter variations between the two years. This latter possibility would be supported by non-overlapping confidence regions in parameter space. Variation in the values of μ_{max} and d_g associated with each K_N and m will also be inspected for systematic changes.

Additional model assessment is provided by calculating the proportion of the log-transformed data variance explained by the model (i.e., the coefficient of determination R^2). This is done for point-to-point comparison and after averaging the log-transformed model output and log-transformed observations over circular areas with increasing radii of 10, 25, 50, and 100 km, and on a cruise-by-cruise basis. This analysis is intended to determine

the scales over which a precise match between model and data is expected. These metrics, being descriptive, do not play a role in parameter estimation and are not used to make detailed statistical inferences.

All surface data are used in the 1993 analysis. However, in 1994, cruise 8 (which is actually a single transect) was omitted because it follows the last reliable estimates of *A. fundyense* at the boundary by over 3 weeks and was sensitive to their specification. In addition, preliminary analysis of cruise 6 in 1994 indicated that the model could not match the magnitude of a large patch of cells observed offshore of Casco Bay. The inclusion of this feature has a strong effect on the likelihood analysis and could not be explained by the large-scale dynamics resolved by the biological model. Its magnitude ($\sim$900 cells/L) suggests it may have originated in the EGOM, which often has large *A. fundyense* populations around the mid-June time period of cruise 6 (Townsend et al., 2001; Keafer et al., 2005), but was not observed at the domain boundary due to the limited sampling. It is thus treated as a misfit *a priori*. This leaves 462 of the 515 observations of *A. fundyense* abundance (90%) to provide active data for the 1994 optimization.

3. Results and discussion

3.1. Physical model

Both the modeled and observed currents at Cape Porpoise flow persistently to the southwest through early June at all depths, with only short time-scale interruptions (Fig. 6). April surface currents are faster and show a greater onshore tendency in 1993 than in 1994. The former are associated with predominantly downwelling-favorable winds, and the latter with greater upwelling (see Fig. 3). In May of 1993, the modeled surface flow is larger than that observed, but both the model and the observations have strong alongshore currents that are maintained through much of June. Modeled surface currents in 1994 are somewhat less than those observed at the surface in both April and May but comparisons at depth are excellent. Currents decrease in magnitude and veer offshore in June 1994 in association with several pronounced upwelling events and a decline in river discharge (Fig. 3).

Comparison of salinity fields in 1993 (Fig. 7, top panel) shows a similar alongshore progression of freshwater and a similar response of the plume to

wind events in the model and observations. Down-welling conditions (cruises 1–2) press the freshwater plume toward the coast and upwelling (cruise 4) spreads it offshore. Modeled surface salinity is, on average, 0.7 ppt greater than that observed but this has not caused a large departure in current strength for 1993 (i.e., Fig. 6) nor does it have a significant impact on the predicted maximal growth rate (Fig. 4(C)). The vernal warming of surface waters is well captured in the model (middle row) and the model thus matches the regional-scale DIN draw-down associated with the spring bloom (bottom row). However, the detailed patchiness in the nutrient field is not captured.

In 1994, both the modeled and observed fresh-water plumes are spread further offshore in late April and early May (cruises 1a and 1b) than in 1993 (Fig. 8, top row) due to the prevalence of upwelling-favorable winds (Fig. 3). The offshore spread of the modeled plume is somewhat greater than that observed and salinity gradients are not as pronounced. This may contribute to slower along-shore flow in the model during May of 1994 (i.e, Fig. 6). On average, the model is 0.5 ppt saltier than the observations. Vernal warming in 1994 is well captured by the model (middle row). The surface temperature during cruises 1a and 1b of 1994 is warmer than that during the same time period in 1993 (i.e., cruise 2 of 1993). The 5–8 °C surface temperatures during these cruises suggest that they followed the spring nutrient drawdown (Figs. 5(A) and (B)). Variance around median DIN values is high in this temperature range (Fig. 5B) and considerable unresolved patchiness is apparent. In June 1994, observed nutrients were low throughout offshore waters but a limited region of elevated DIN is apparent near the coast, associated with strong upwelling favorable winds during this period (i.e., Fig. 3). The near-shore modeled surface waters cool in response to this upwelling (Fig. 8, cruise 5a). However, the temperature change is small relative to the dominant vernal warming signal in the nutrient function and the observed near-shore region of elevated DIN is thus not captured.

In summary, the physical model captures the persistent southwesterly flow of the WMCC during 1993 and 1994 both at the surface and at depth. The vernal warming of surface waters, which influences *A. fundyense* growth both directly by temperature effects (Fig. 4(D)) and indirectly through the associated nutrient depletion (Figs. 5(A) and (B)), is also well captured. The mechanistic response of
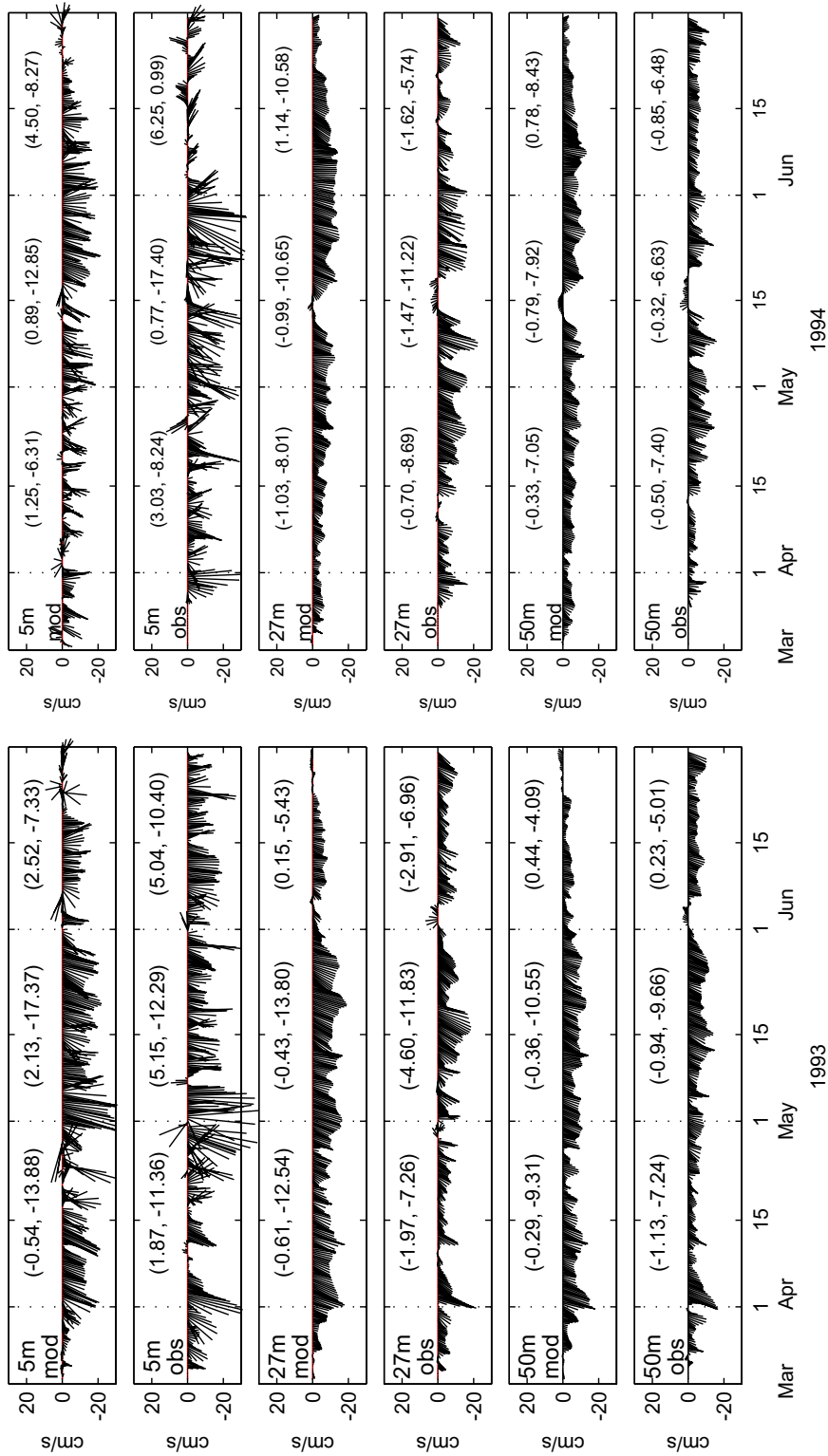
Fig. 6. Comparison of the modeled (mod) and observed (obs) current velocities at the Cape Porpoise offshore mooring site (Fig. 1, site P2 of Geyer et al. (2004)) for 1993 (left panel) and 1994 (right panel). Values listed in parentheses are the mean along-shore and cross-shore velocities for April, May, and June. The along-shore is defined as 30° east of true north.
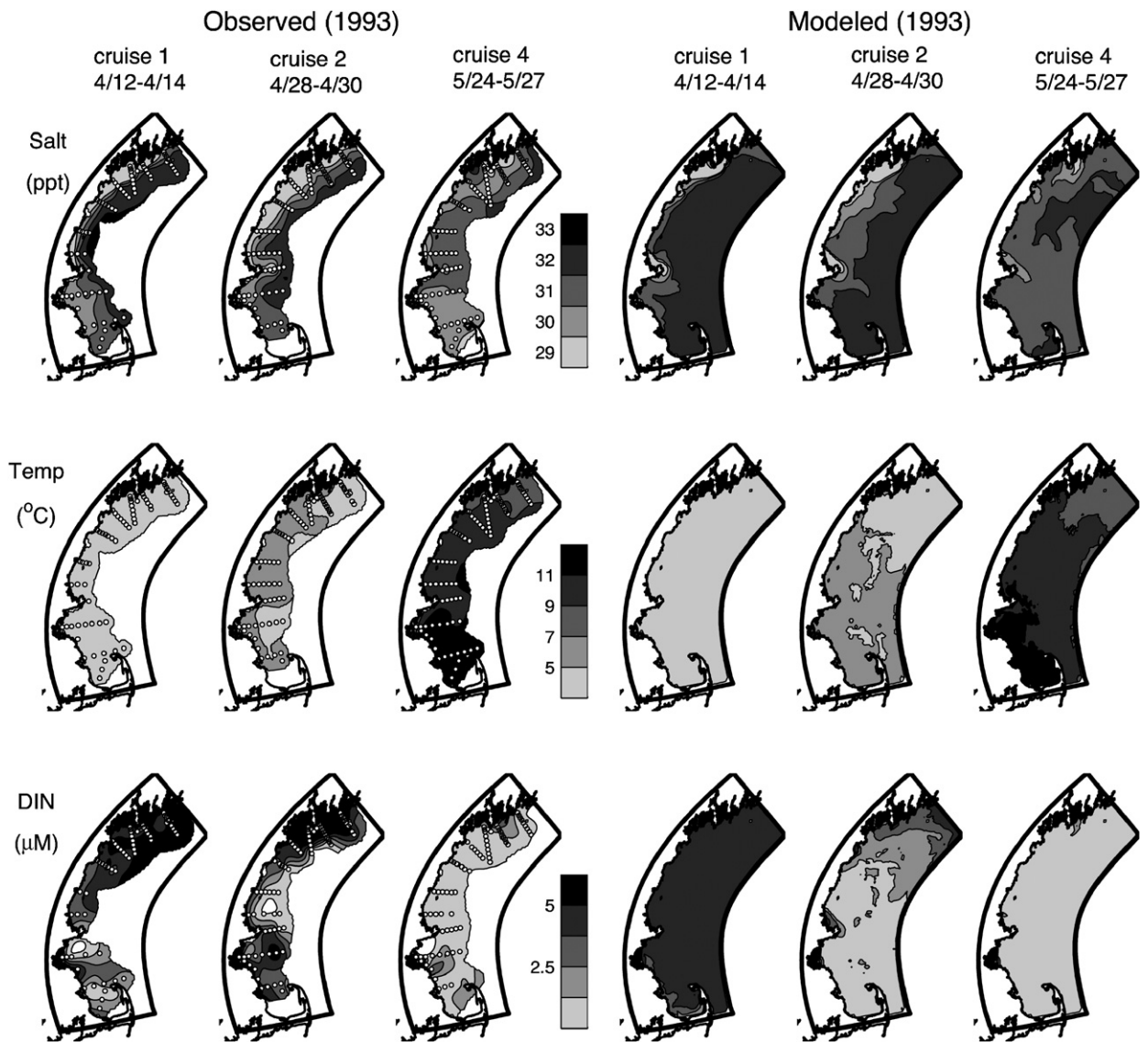
Fig. 7. Comparison of observed (left) and modeled (right) surface salinity (top row), temperature (middle row), and DIN (bottom row) for selected cruises in 1993. Observation locations are marked by open dots.

river plumes to fluctuations in wind is apparent in the model, but the strength of the river plumes is somewhat underestimated. This has not severely compromised the modeled currents and biases of 0.5–0.7 ppt have a minor influence on *A. fundyense* growth (Fig. 4(D)) and nutrient levels (Figs. 5(A) and (C)). Resolution of nutrient dynamics is restricted to capturing the regional scale seasonal drawdown, but not the detailed patchiness. The potential impact of this patchiness will be discussed further in Section 4.

3.2. Biological model optimization

3.2.1. 1993 Optimization: a match to the large-scale features of the observed bloom

Results of the parameter optimizations for 1993 and 1994 are summarized in Fig. 9. The first two columns show the values of μ_{max} and d_g that yield the maximum likelihood (i.e., best fit) for each choice of K_N (abscissa) and m (ordinate). The third column contours the likelihood associated with these combinations of biological model parameters.
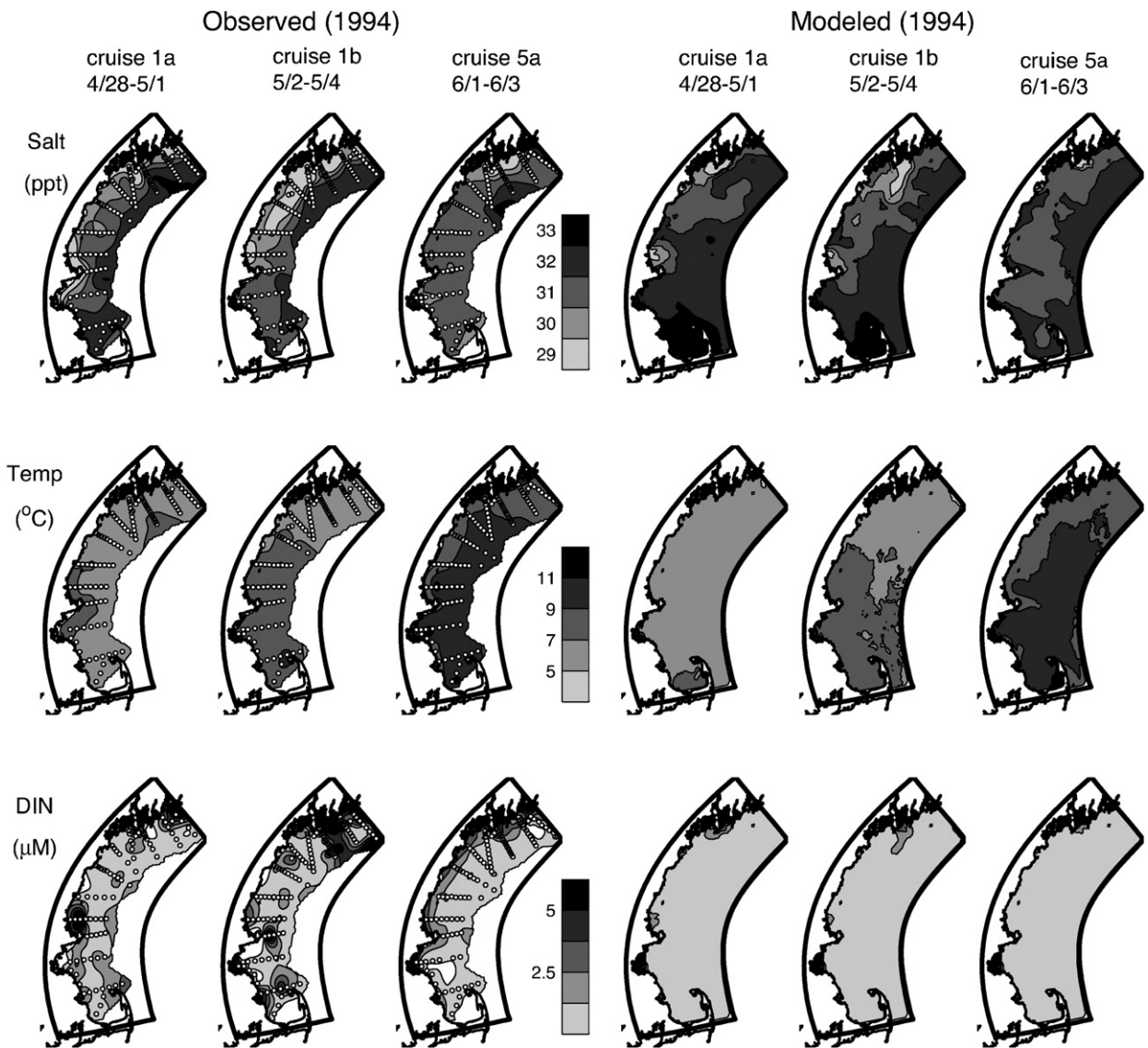
Fig. 8. Comparison of observed (left) and modeled (right) surface salinity (top row), temperature (middle row), and DIN (bottom row) for selected cruises in 1994. Observation locations are marked as open dots.

The *overall* best fit for 1993 occurs at $K_N = 1.0\,\mu M$ and $m = 0.10\,\mathrm{day}^{-1}$ (circled), with $\mu_{max} = 0.70$ (left column) and $d_g = 0.75\,\mathrm{cm}$ (center column). An area of elevated likelihood surrounds this optimal parameter combination. Confidence regions (gray lines) show that the model/data comparison cannot strongly differentiate the skill attained by the optimal parameter values from that obtained using a range of alternative combinations. As values of K_N and m increase, higher values of μ_{max} and d_g are invoked to obtain the best fit (i.e., moving up and to the right in columns 1 and 2). At very large K_N and m, the likelihood decreases significantly. Strong

losses and growth limitation via nutrients in this part of parameter space cause the modeled bloom magnitude to lag behind observations (not shown) despite high μ_{max} and d_g. The likelihood also decreases sharply with very low m and K_N, as not even the lower limits of μ_{max} and d_g can prevent the modeled bloom from reaching concentrations well beyond observations (e.g., the baseline $m = 0\,\mathrm{day}^{-1}$, $K_N = 0\,\mu M$ case described in detail by Stock et al. (2005)). The results of the 1993 optimization have changed little from those presented in Stock et al. (2005) (Fig. 9, middle row). The 90% confidence contour now closes just before $K_N = 0\,\mu M$ and
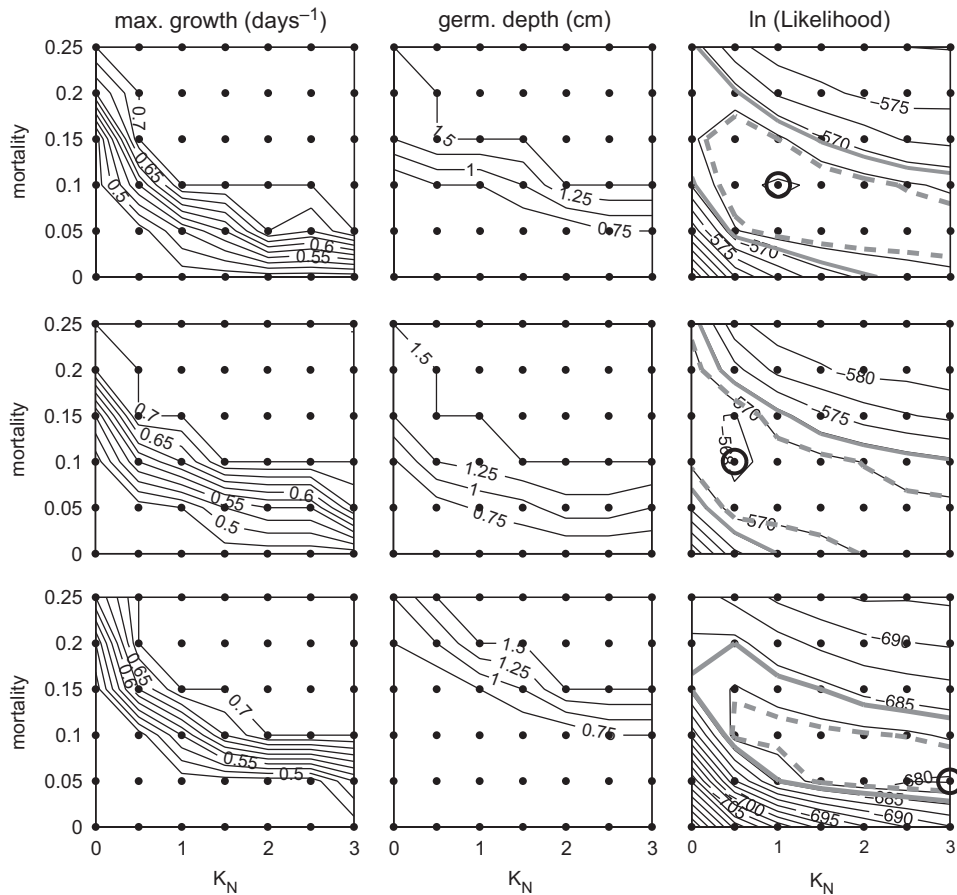
Fig. 9. Model optimization results for 1993 (top row), optimization results for 1993 in Stock et al. (2005) (middle row), and for 1994 (bottom row). The left and center columns give the values of μ_{max} and d_g associated with the best runs for each value of K_N and m, the right column gives the likelihood. In the right column, the thick, gray dashed line is the 90% confidence region around the best combination of K_N and m (circled), and the thick gray solid line is the 99% confidence region. Note that the likelihood is the product of probabilities of each misfit, and thus scales inversely with the number of observations. Assessment of the relative performance in 1993 and 1994 is thus done through misfit properties when the likelihood has been maximized (i.e. Tables 4 and 5), not the likelihood itself.

$m = 0\,\text{day}^{-1}$ axes and optimal parameter values have shifted slightly, but the basic features are similar.

Comparison of the observed and modeled *A. fundyense* distributions for the optimal simulation in 1993 (Fig. 10) reveals similarities in the timing, magnitude, and alongshore progression of cells over large spatial scales. The *e*-folding scale of the remaining misfit ($1/r_x$, $1/r_y$, Table 4) is 15–20 km in both the alongshore and crossshore directions, suggesting that small-scale misfits dominate the remaining unexplained variance. The calculated R^2 metrics (Table 4) show that the model captures little of the point-to-point variance, but explains much of the variance between cruises and after averaging over large spatial scales. The R^2 metrics for

simulations from either end of the confidence regions in Fig. 9 (i.e., Table 4, low K_N, high m; high K_N low m) are similar to those for the optimal run (i.e., 1993 best). Values have improved slightly relative to the best simulation from Stock et al. (2005, Table 4, last column).

3.2.2. 1994 Optimization: evidence of a model deficiency

The 1994 optimization has a region of elevated likelihood similar to that for 1993 and similar trends in μ_{max} and d_g (Fig. 9, bottom panel). The optimal simulation in 1994 has $K_N = 3.0\,\mu\text{M}$, $m = 0.05\,\text{day}^{-1}$ and calls for a smaller cyst source ($d_g = 0.5\,\text{cm}$) and lower maximum growth ($\mu_{max} = 0.525\,\text{day}^{-1}$) than the 1993 optimization (Fig. 9,
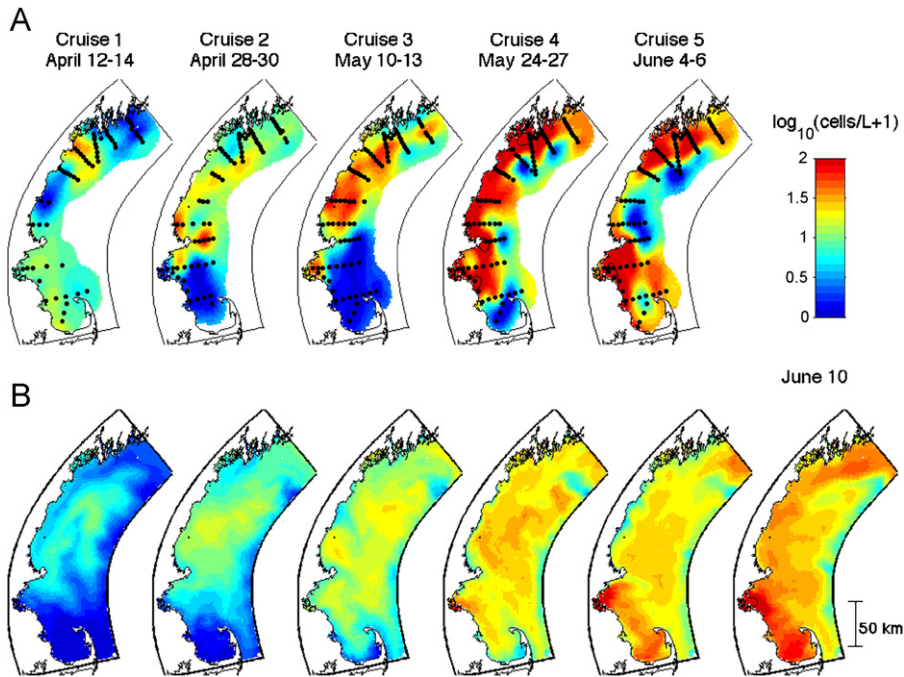
Fig. 10. The 1993 model/data comparison. (A) The observed surface *A. fundyense* cell distribution. (B) The modeled cell distribution for the 1993 best simulation ($K_N = 1.0\,\mu M$, $m = 0.1\,day^{-1}$). Note that the color scale in Figs. 10 and 11 is chosen to capture variation in the majority of the data (91% of measurements are < 100 cells/L). Areas with concentrations > 100 cells/L are shown in dark red. Black contours within these areas indicate isolated patches with > 200 cells/L (3% of points). While there are no *A. fundyense* observations for June 10, the model results are shown as it is immediately before the period of peak shellfish toxicity (Fig. 2) and will be discussed within the model diagnosis (Section 3.3).

Table 4
Summary of optimal model parameters and misfit statistics for optimizations to 1993 data (variance of observations is 2.60)

	1993 Best	1993, Low K_N, high m	1993, High K_N, low m	1993 Best Stock et al. (2005)
μ_{max} (day^{-1})	0.700	0.700	0.700	0.575
d_g (cm)	0.75	1.50	0.75	1.25
m (day^{-1})	0.1	0.15	0.05	0.1
K_N (μM)	1.0	0.5	3.0	0.5
log(L)	−564.7	−565.1	−565.7	−567.7
Misfit variance[a]	2.15	2.21	2.22	2.34
σ^2 (*fit by likelihood*)	2.34	2.35	2.41	2.51
r_x (km^{-1})	0.0597	0.0594	0.0579	0.0541
r_y (km^{-1})	0.0606	0.0612	0.0581	0.0566
r_t (days^{-1})	0.128	0.125	0.128	~0.127[b]
R^2 results				
Point to point	0.18	0.15	0.15	0.10
10 km scales	0.25	0.23	0.21	0.17
25 km scales	0.37	0.36	0.32	0.23
50 km scales	0.55	0.56	0.47	0.31
100 km scales	0.69	0.70	0.66	0.49
Cruise by cruise	0.83	0.84	0.85	0.68

[a]Note that two variances are reported. The first is associated with the raw variance of the misfits. The second is the variance fit via maximum likelihood. The small difference reflects the likelihood's accounting for correlation in space and time in its calculation.
[b]Converted from discrete estimate of Stock et al. (2005) (see Section 2.4).

Table 5
Misfit properties for 1994 simulations

	1994	1994 With 93 best parameters	1994 With 93 high m, low K_N	1994 With 93 high K_N, low m
μ_{max} (day^{-1})	0.525	0.700	0.700	0.700
d_g (cm)	0.50	0.75	1.50	0.75
m (day^{-1})	0.05	0.1	0.15	0.05
K_N (μM)	3.0	1.0	0.5	3.0
log(L)	−679.7	−689.1	−692.8	−687.5
Misfit variance	1.90	2.10	2.20	2.08
σ^2 (fit by likelihood)	2.09	2.32	2.50	2.25
r_x (km^{-1})	0.0767	0.0690	0.0634	0.0715
r_y (km^{-1})	0.0597	0.0560	0.0511	0.0577
r_t (days^{-1})	0.872	0.945	0.972	0.897
R^2 results				
Point to point	0.16	0.07 (0.22)	0.03 (0.18)	0.08 (0.18)
10 km scales	0.24	0.14 (0.31)	0.09 (0.27)	0.15 (0.26)
25 km scales	0.38	0.26 (0.48)	0.23 (0.46)	0.26 (0.42)
50 km scales	0.59	0.46 (0.70)	0.46 (0.70)	0.50 (0.63)
100 km scales	0.58	0.46 (0.75)	0.46 (0.78)	0.52 (0.69)
Cruise by cruise	0.62	−0.11 (0.85)	−0.09 (0.88)	0.26 (0.76)

The variance of observations = 2.26

Table 5). However, the modeled *A. fundyense* bloom with these settings underestimates observations throughout May and early June (Figs. 11(A) and (B)). This moderate bias over large scales is not strongly reflected in the point-to-point variance, which is dominated by small-scale patchiness (Table 5, $1/r_x$ and $1/r_y \sim 15$–20 km). The R^2 metrics after averaging over larger spatial scales, however, are lower than those achieved for 1993 (Table 5 compared to Table 4) and bias is clearly evident in the cruise-averaged comparisons (Fig. 12). For 1993 (Fig. 12, top panel), the modeled mean *A. fundyense* abundance from simulations spanning the confidence region in Fig. 9 are somewhat lesser than that observed during cruise 1, but track observations closely thereafter. In 1994 (bottom panel), the optimal simulation starts with approximately the right mean abundance, but then underestimates observations over the next 5 cruises before converging again by cruise 7.

There is evidently a deficiency in the model dynamics and/or forcing that prevents matching both the rise of *A. fundyense* abundance from May to early June (i.e., bloom development), and the sharp decline in abundance in MB/CCB in mid-June of 1994 (i.e., bloom termination). The optimization lessens the severe misfit during cruise 7 by imposing a moderate bias during May and June. Marked overestimation of the observed cell abundance

during cruise 7 in simulations that do not invoke both mortality and nutrient dependence (not shown) is primarily responsible for the strong rejection of such simulations of the 1994 data (Fig. 9, bottom right panel).

3.2.3. 1994 Simulation with 1993 parameters: a large-scale match until mid-June

Running the 1994 simulation with 1993 parameters increases the model/data misfit in MB/CCB during cruise 7 (i.e., bloom termination), but improves the fit earlier in the spring (i.e., bloom initiation and development, Figs. 11(C) and 12). The larger cruise 7 misfit decreases the likelihood and R^2 metrics relative to the optimal 1994 simulation (Table 5), but the R^2 values for data until cruise 7 are comparable to values in 1993 (Table 5, values in parentheses). The modeled *A. fundyense* cells during cruises 1a and 1b are located offshore and somewhat downstream of those observed (Fig. 11(A) versus (C)). These cells arise mainly from the germination of cysts offshore of Casco Bay in the model and the spatial misfit may be related to unresolved spatio-temporal variability in the cyst source (discussed further in Section 4). Apart from this moderate spatial mismatch, the changes in mean bloom magnitude and the large-scale aspects of the alongshore progression of *A. fundyense*
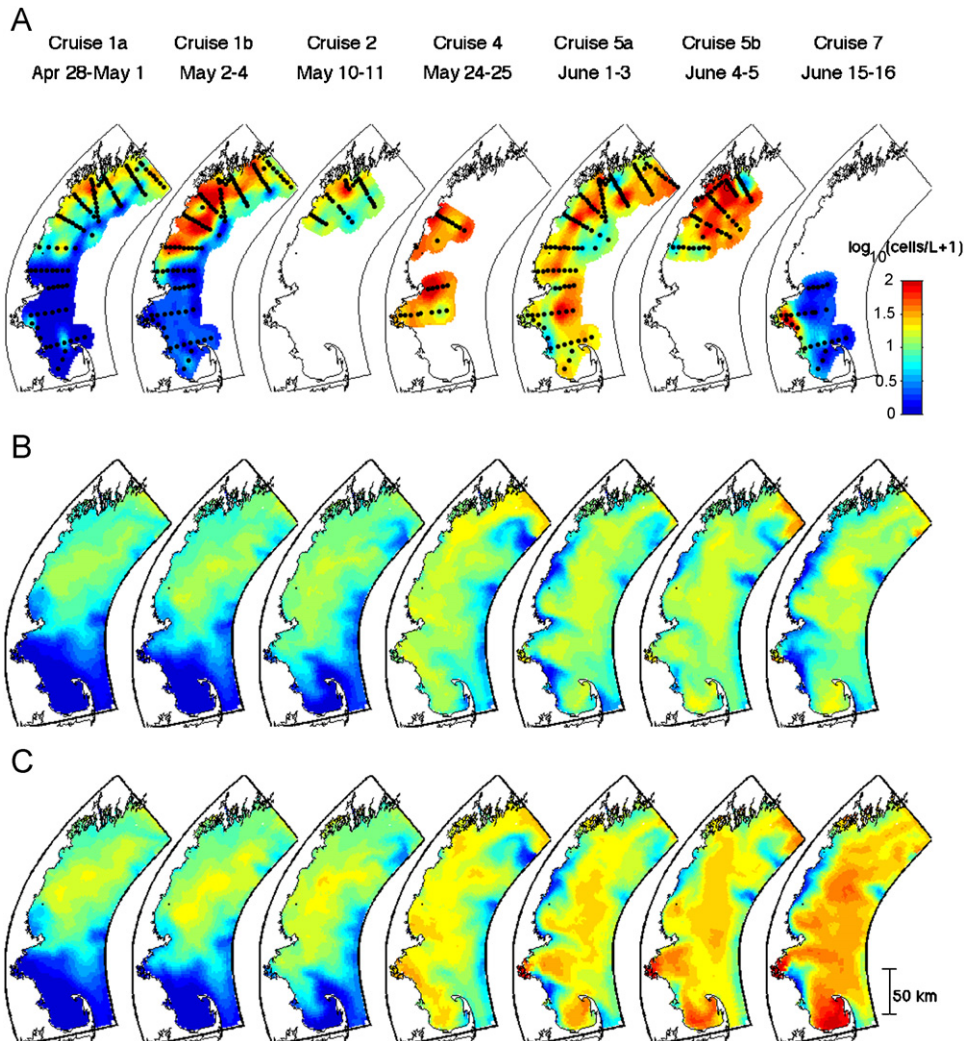
Fig. 11. The 1994 model/data comparison. Contours are as in Fig. 10. (A) The observed surface *A. fundyense* cell distribution. All active data cruises are shown except cruise 3 (only 9 observations). (B) The modeled cell distribution for the 1994 best simulation ($K_N = 3.0\,\mu M$, $m = 0.05\,\text{day}^{-1}$). (C) The modeled cell distribution resulting from the 1994 simulation with best parameter values derived in 1993 ($K_N = 1.0\,\mu M$, $m = 0.10\,\text{day}^{-1}$).

(i.e., the introduction of cells into MB/CCB by late May) are captured by the model until cruise 7.

The similar performance of the 1993-based model parameters through bloom initiation and development during both years offers little evidence that changes in biological model parameters contributed to large-scale differences in bloom properties. However, the model-data disparity in Massachusetts and CCB in mid-June suggests that additional resolution of the dynamics underlying bloom termination is necessary.

3.3. Diagnosis of model solutions

The diagnosis focuses on several aspects of the model solutions: (1) outlining the basic properties of those simulations able to match the large-scale observed *A. fundyense* bloom patterns through mid-June (i.e., the best-fit 1993 solutions), (2) identifying the dynamics underlying the departure of these simulations from observations in mid-June 1994 in MB/CCB, and (3) searching for plausible explanations for the large differences in shellfish toxicity between the 2 years. This is approached by first
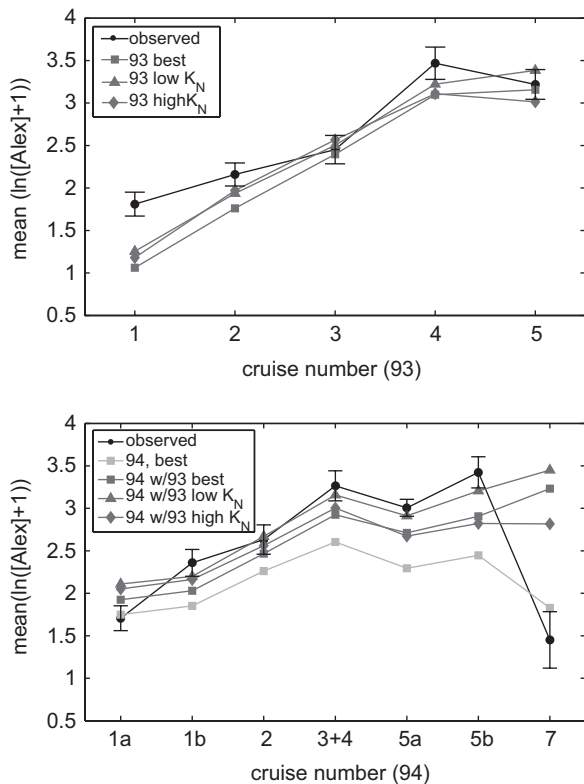
Fig. 12. Top panel: Cruise-by-cruise model-data comparison for a range of optimally performing simulations in 1993. Error bars are standard deviations around the mean of the observed sample for each cruise. Bottom panel: Cruise-by-cruise comparison for the optimal simulation in 1994, and for 1994 simulations run with 1993 derived parameter values.

focusing on domain-averaged patterns and then on patterns in the Northern (Casco Bay) and Southern (MB/CCB) regions of the domain. Generally, only results from simulations using the best-fit parameter values from 1993 are shown. Where deviations exist over the range of parameter uncertainty, they will be mentioned in the text.

3.3.1. Domain-wide patterns: cysts near Casco Bay and limited net growth

The total number of cells in the model domain in 1993 and 1994 are similar through early June (Fig. 13(A)). This is supported by the observations (i.e., Figs. 10–12). Neither simulation requires large average net growth rates (Fig. 13(B)) to account for observed changes in the mean abundance over large scales through early June. This remains true for all parameter values within the confidence intervals. The maximum change in cell numbers via net growth relative to the cells produced by cyst

germination and EGOM inflows is roughly a factor of 2 through early June.

Domain-averaged modeled net growth rates remain low throughout the spring in both years due to a combination of low temperatures early in the spring (Fig. 13(C)) low nutrients after the spring bloom (Fig. 13(D)) and losses via mortality. The model/data comparison has difficulty determining the relative importance of these two latter factors (i.e., note the size of confidence regions in Fig. 9), but the best simulations use a combination of both. The strong negative correlation between nutrients and sea surface temperatures minimizes the impact of differences in the timing of vernal warming between 1993 and 1994 on net growth rates. That is, though waters warm faster in 1994 (favoring growth), nutrients deplete more quickly (slowing growth) resulting in similarly low net growth during both years.

The increase in net growth rates after June 1 during both years results from differences in the temperature dependence of the growth rate (which peaks at $\sim$15–18 °C, Fig. 4(D)), and the temperature dependence of DIN (which reaches its minimum near $\sim$5 °C, Fig. 5). Minimum nutrients are 0.7 μM. Thus, even with $K_N = 3.0$ μM, *A. fundyense* cells are able to attain a modest fraction ($\sim$10%) of their maximum growth rate with nutrients at minimum levels. As the maximum attainable growth rate continues to rise in warming waters, constant mortality is overcome and a modest positive growth rate in mid-June results. This contributes to the model's difficulty capturing the decline of cell abundances in MB/CCB in mid-June of 1994 (discussed further below).

Breaking down the modeled cell population by the origin of the parent cells (Figs. 13(E) and (F)) reveals a similar composition for the two years. It also suggests the overall importance, in a domain-averaged sense, of cells derived from the germinating cysts in the deep cystbed (>50 m) offshore of Casco Bay. Cells derived from cysts germinating in shallow waters accounted for $<10\%$ of the cells in the domain at any time. The contribution of cells from the EGOM is very small in April, but rises steadily in May until cells of EGOM origin (or their offspring) account for $\sim$30% of the total cell abundance.

3.3.2. Diagnosis of bloom patterns in the Casco Bay region

While the model cannot simulate the precise placement of patches on smaller spatial scales, it is
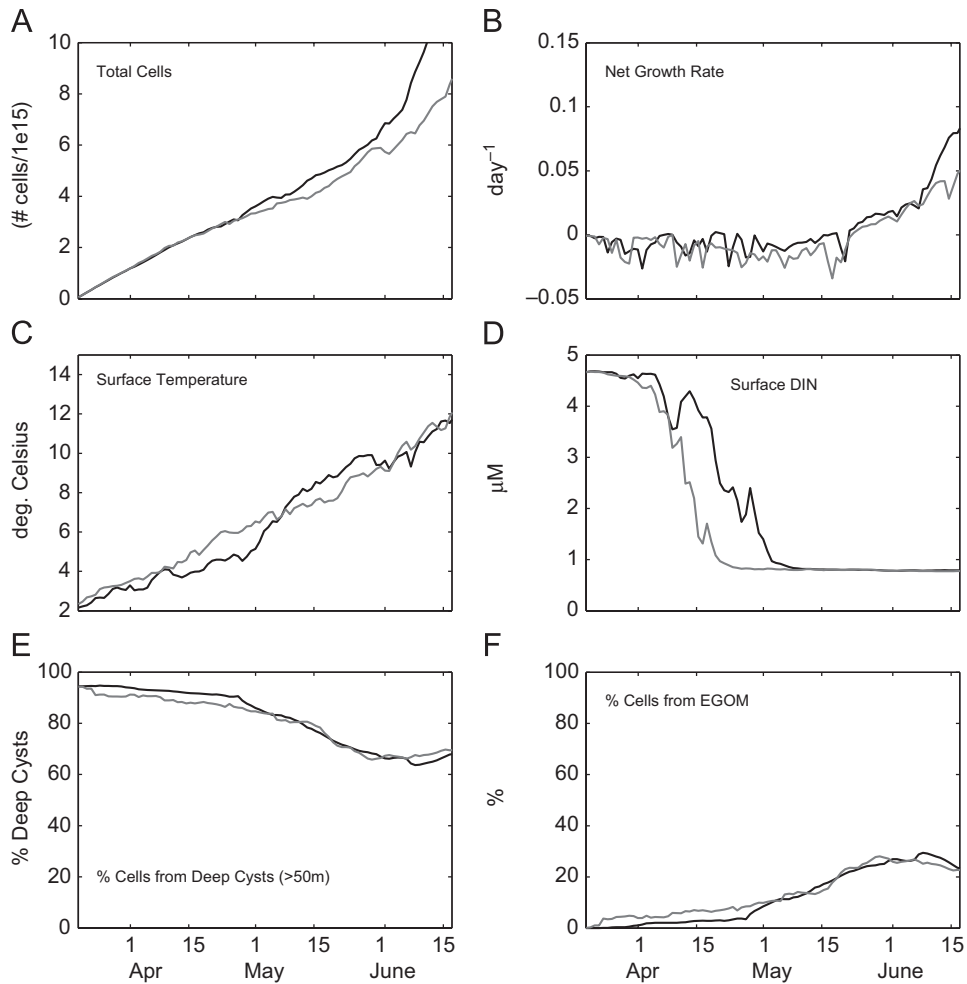
Fig. 13. Comparison of domain-averaged physical and biological quantities for 1993 (black lines) and 1994 (gray lines). Note that the net growth rate in panel B is that which results from the maximum rate at a given temperature and salinity (i.e., Fig. 4(D)) modified by nutrient and light limitation, and mortality.

possible to make generalizations about cell populations and gain mechanistic insight into the factors influencing *A. fundyense* populations in the Casco Bay region (Fig. 1). The model generally predicts a similar number of cells in the Casco Bay region during both years until early June (Fig. 14, top panel). This is largely corroborated by cruise data, although peak concentrations in the model are lower than the observations (i.e., Figs. 10 and 11). A larger percentage of the modeled cells in this region are from the EGOM and shallow cysts (Fig. 14, middle panel) relative to the domain average (Fig. 13, bottom panel). This is due to Casco Bay's proximity to these sources and because many cells germinating in offshore waters in the model are advected to the south by the WMCC before influencing Casco Bay.

The largest difference in modeled cell abundance in the Casco Bay region occurs from June 5 to 15 and coincides with the most prominent difference in shellfish toxicity between the 2 years (Fig. 2). A strong downwelling wind event from June 5 to 10 of 1993 (i.e., Fig. 3) causes an influx of cells (Fig. 14, bottom panel) of EGOM origin (Fig. 14, middle panel). This is also apparent in the June 10, 1993 modeled cell distribution (Fig. 10, bottom right panel). In 1994, winds were upwelling favorable throughout much of June, and toxicity was much lesser despite similar observed cell abundances prior to June 5. The peak in 1993 shellfish toxicity in Casco Bay unfortunately follows the last *A. fundyense* observations by approximately 1 week. However, the close coincidence between strong downwelling and the toxicity peak, along with a
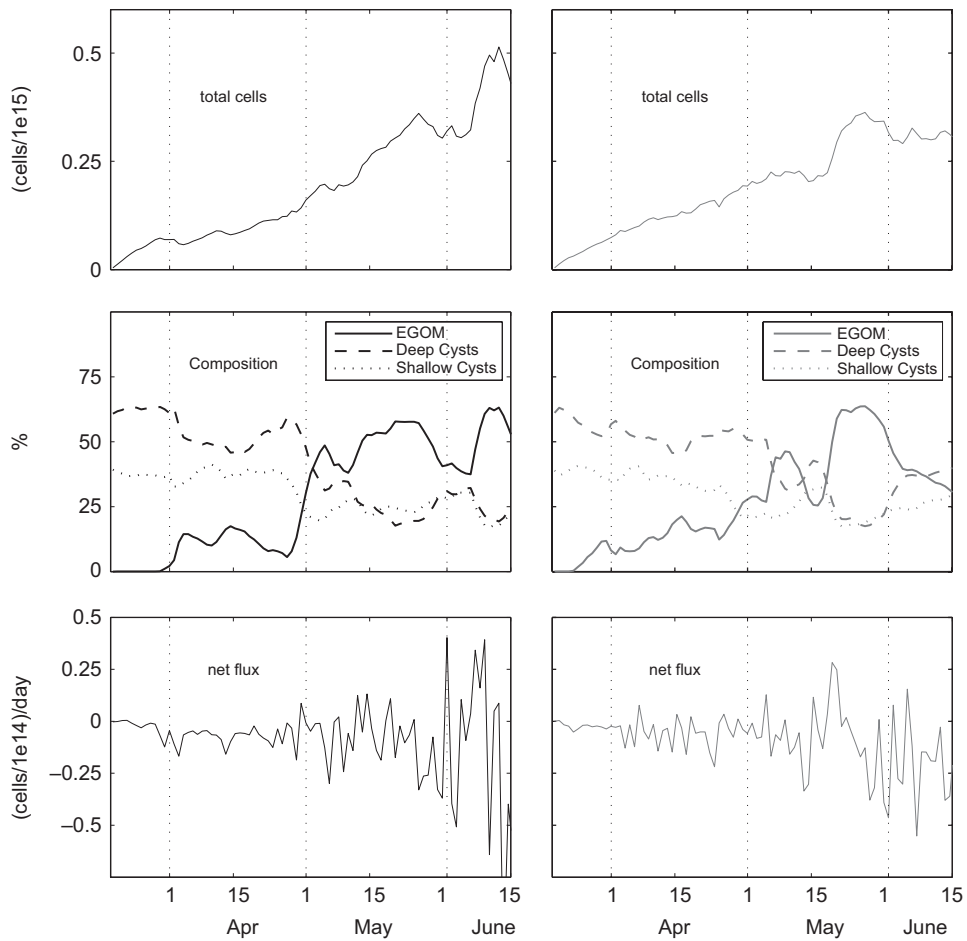
Fig. 14. The Casco Bay cell budget for 1993 (left panel) and 1994 (right panel). Top panel is the total cells in the region. Middle panel is the percentage of cells in the region that originated (or whose parent cells originated) from each of three different sources. Bottom panel is the net influx (positive values) or outward flux (negative values) of cells from the region.

clear mechanism and contrast with 1994, is suggestive of causal link.

3.3.3. Diagnosis of bloom patterns in Massachusetts and Cape Cod Bays

The cell budgets for MB/CCB in 1993 and 1994 are shown in Fig. 15. In 1993, low cell populations are within MB/CCB by mid-April, following strong downwelling winds and rapid alongshore flows early in the month (Fig. 15, top panel). Upwelling in April 1994 slows alongshore transport, but does not prevent it (i.e., see mooring comparison in Fig. 6). The introduction of cells to MB/CCB is thus delayed relative to 1993, but both the model and the observations support the presence of substantial cells in the region by late May (Figs. 10 and 11). The modeled *A. fundyense* populations in MB/CCB during both years are dominated by cells originating

from cysts in the offshore cyst seedbed near Casco Bay or their offspring (Fig. 15, middle panels), with only a small contribution from the EGOM.

As in the coastal region near Casco Bay, influxes are associated with downwelling winds (e.g., bottom panel of Fig. 15, May 29–30 and June 5–10, 1993, May 15–20, 1994). Periods of upwelling, in contrast, are associated with net fluxes out of the region (e.g., June 1–2, 1993; June 1, 6, and 15 of 1994). Increasing net growth rates (i.e., Fig. 13(B)) cause cell numbers to rise in June during both years despite marked outward fluxes in 1994 associated with upwelling winds. This contributes to the model's difficulty matching the observed decline of cell abundance in the region during Cruise 7 (June 15–17).

Differences in wind forcing also influence the distribution of *A. fundyense* within MB/CCB
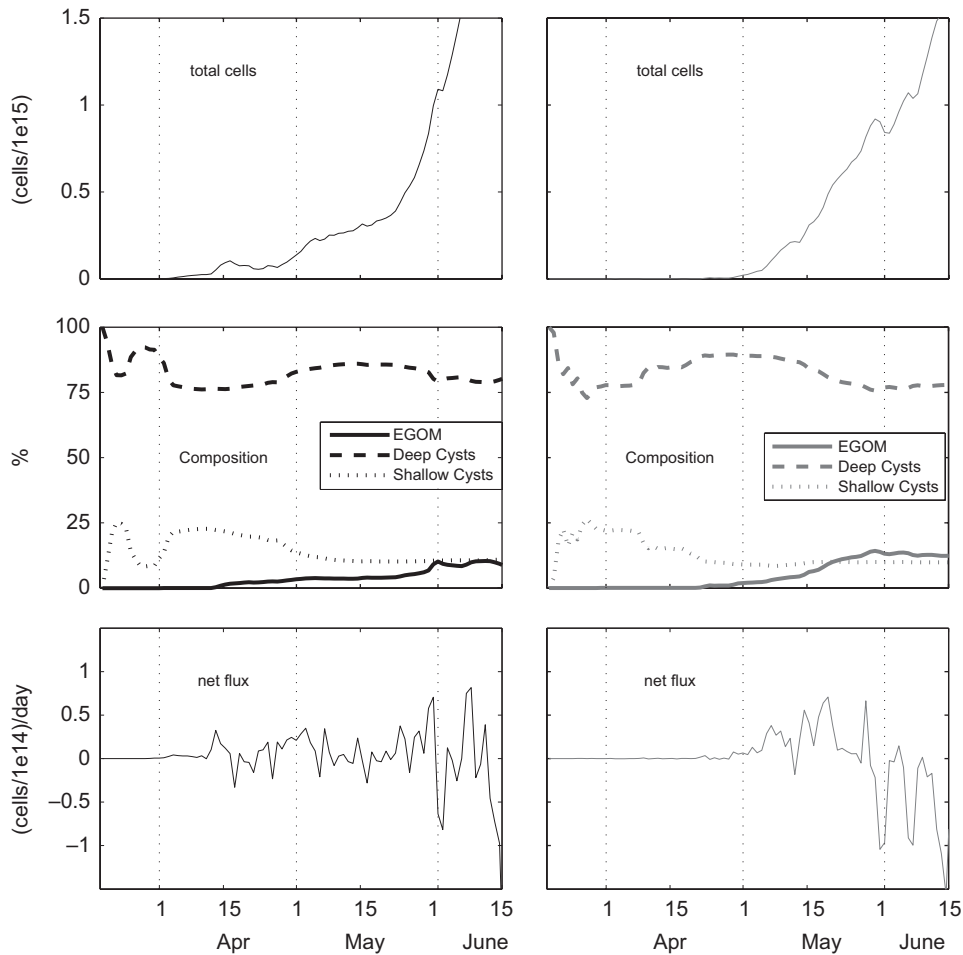
Fig. 15. MB/CCB cell budget. Panels are as in Fig. 14.

(Fig. 16). Modeled bloom patterns in the region are similar during both years on May 28. This is supported by late May observations (Figs. 10 and 11) although only a MB transect was occupied during this period in 1994. By May 30 of 1993, strong downwelling winds have pushed cells against the south coast of Massachusetts in the model, coinciding with rising shellfish toxicity at Cohasset and Scituate (Fig. 2). On June 6–8, a second downwelling event transports *A. fundyense* to the coast, and a second toxicity rise reaching as far south as the Cape Cod Canal station results. The proximity of cells to the coast during this period is well supported by MB/CCB observations on June 6 (Fig. 10). In 1994, upwelling in early June creates a gap between the coast and modeled *A. fundyense* populations and no toxicity is observed within MB/CCB. This gap is well supported by the June 1–3

cruise data (Fig. 11). However, cells in eastern CCB in the model are not effectively flushed from the region during upwelling. This result combines with positive net growth in June (Fig. 13(B)) to prevent the model from matching the low observed cell abundance in much of MB/CCB on June 15–16 1994.

4. Conclusions

In 1993, observations covered the initiation and development of *A. fundyense* blooms in the WGOM. The model is able to capture the large-scale aspects of the observed 1993 bloom using a range of nutrient dependence and mortality. In 1994, observations covered bloom initiation, development, and, in MB/CCB, bloom termination. Simulations capturing the initiation and
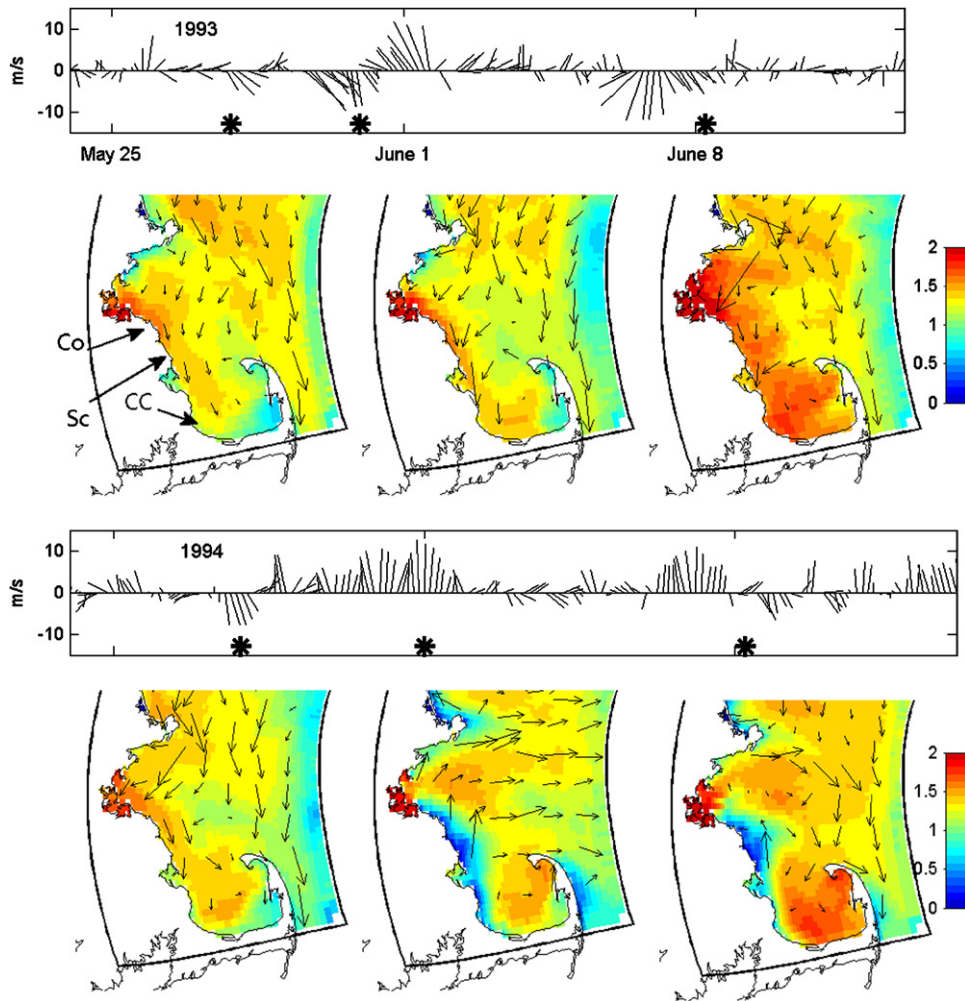
Fig. 16. Winds and the spatial distribution of *A. fundyense* in MB/CCB during late May and early June of 1993 (top panels) and 1994 (bottom panels) for simulations with optimal 1993 settings. Asterisks on the wind panel mark the times for which model output is shown. "Co", "Sc", and "CC" on the upper left panel refer to the Cohasset, Scituate, and Cape Cod Canal toxicity stations, respectively (i.e. Fig. 2).

development of the bloom in 1994 do not capture bloom termination, suggesting the need for further resolution of termination dynamics (see below). In the 1994 optimization, this deficiency is manifested as a moderate negative bias during bloom initiation and development and a moderate positive bias at termination.

Diagnosis of simulations matching large-scale patterns during bloom initiation and development for both years (i.e., those with 1993-derived para-meter values) provides little evidence that changes in biological dynamics acting over regional and seasonal scales were primary drivers of differences in shellfish toxicity. However, the potential impact of biological dynamics and forcing acting over small

scales is not well assessed by this model and may be important. Variations in *A. fundyense* transport linked to June wind forcing are suggested as a plausible explanation for the major differences in shellfish toxicity between the 2 years. The plausi-bility of this explanation is contingent upon two robust elements of the model well supported by the data: (1) a persistent southwesterly flowing WMCC (Fig. 6), that is responsible for the similar along-shore extent of *A. fundyense* populations by late May of both years (Figs. 10 and 11), (2) a strong influence of upwelling and downwelling winds on crossshore transport in surface waters (i.e., Figs. 7 and 8 for river plumes, Figs. 10 and 11 for cells, see also Geyer et al., 2004 and Fong et al., 1997).

The suggested physical explanation for differences in shellfish toxicity in the WGOM during 1993 and 1994 is generally consistent with prior hypotheses (e.g., Franks and Anderson, 1992a, b; Anderson et al., 2005a). However, the large-scale, barotropic component of the WMCC plays a prominent role in the alongshore transport of *A. fundyense* cells (see also Geyer et al., 2004). This diminishes the importance of local river inputs in determining the alongshore extent of *A. fundyense* cells and shellfish toxicity in 1993 and 1994 (i.e., Franks and Anderson, 1992b). In addition, while upwelling in April and May of 1994 slowed the alongshore transport of *A. fundyense* and likely influenced shellfish toxicity during this period (i.e., Anderson et al., 2005a), the persistent large-scale circulation ensured a similar alongshore extent of cells by late May of both years.

The suggestion that mean upwelling in April and May does not necessarily prevent outbreaks of shellfish toxicity in June, even in regions as far south and west as MB/CCB, has important consequences for managers. The problem becomes one of identifying critical periods when strong downwelling events are likely to create the largest toxicity response in shellfish. In 1993 and 1994, the late May and early June period of high cell abundance is suggested as particularly critical. Toxicity records suggest this is a persistent period of risk in both regions (Franks and Anderson, 1992b; Luerssen et al., 2005). Storm events, particularly "nor'easters" with strong downwelling winds, become less common as spring turns to summer (Zielinsky and Keim, 2003), suggesting the potential importance of somewhat anomalous storm events for large PSP outbreaks in June and July.

Given these results, it is interesting that historical WGOM shellfish toxicity records analyzed by Franks and Anderson (Franks and Anderson, 1992b) showed a robust positive correlation between the southern extent of shellfish toxicity and the May outflow of the Kennebec and Androscoggin rivers. This correlate argues for greater southward progression of toxicity in 1994 (i.e. Fig. 3), yet the opposite occurred. There are several possible explanations for this. First, Franks and Anderson do suggest an increased importance of wind forcing for transport past the Cape Ann branch point because river plumes can separate from the coast after redirection by the land mass. Second, strong downwelling winds in coastal areas of the WGOM can be associated with rainfall-generating atmospheric low-pressure systems (e.g., nor'easters) passing offshore to the south and east, suggesting that downwelling winds and WGOM river inputs may often be correlated.

There are several processes that are unresolved or have limited resolution in the present model that may influence these findings and explain some of the model/data misfits. One is interannual variability in cyst distribution and abundance (Anderson et al., 2005c). For example, a shift in the cyst distribution to the north and inshore in 1994 could account for the mismatches in the modeled and observed cell abundances during cruises 1a and 1b (Fig. 11).

The second uncertain element is limited constraint of cell abundance along the EGOM boundary. The presence of *A. fundyense* cells along this boundary is essential for the plausibility of the explanation offered herein for differences in shellfish toxicity in the Casco Bay region in June of 1993 and 1994. Cells were observed near this boundary in June of both years (20–40 cells/L in 1993 on June 4, and 8–78 cells/L in 1994 on June 1). However, concentrations between 100 and 500 cells/L have been reported near the Penobscot Bay branch point during this time (Townsend et al., 2001; Keafer et al., 2005). It is unclear if populations of this magnitude were present in 1993 and 1994. However, cells were present, there is a clear mechanism for delivery, and growing evidence for a close connection between toxicity in Casco Bay and the transport of cells from the EGOM (Keafer et al., 2005; Luerssen et al., 2005). Modeled cell populations in MB/CCB in contrast, are relatively insensitive to this boundary condition (i.e., Fig. 15).

A third limitation is limited resolution of small-scale biological and physical processes. These include limited resolution of nutrient patchiness (i.e., Figs. 7 and 8), the lack of spatiotemporal resolution of mortality processes, and coarse resolution of inshore regions with complex coastlines such as Casco Bay. While this study has offered a plausible explanation for the differences in shellfish toxicity based on large-scale patterns, small-scale processes cannot be ruled out. Diagnosing small-scale processes and assessing their impacts requires increased physical model resolution in inshore regions and a more complete ecosystem model to mechanistically understand small-scale biological variability. However, evaluating such a models at small scales requires observations of multiple ecosystem components with increased spatiotemporal resolution.

Each of these elements of the uncertainty may contribute to the more prominent misfits in the model. The largest of these is the model's inability to recreate the decline of cell abundance in Massachusetts and Cape Cod Bays in mid-June of 1994. The highest modeled cell abundance within MB/CCB at this time is along the southern and eastern sections of Cape Cod Bay. The ability of upwelling favorable winds to flush cells from this region in the model is limited. Drifter observations support this retentive property, suggesting that summer residence times as long as 20–50 days (Geyer et al., 1992). This retentive property combines with increasing net growth in the model (i.e., Fig. 13) to prevent the model from matching the observed decline in cell abundance. One possible explanation for this misfit is thus unresolved spatial and temporal variation in cell mortality, which includes several processes with limited constraint in the present model (e.g., encystment, and spatial variability in grazing and cell death). Better understanding of these loss processes may yield more insights into the origin of this misfit and to the processes governing bloom termination more generally.

Appendix A. Supporting material

Supplementary data associated with this article can be found in the online version at doi:10.1016/j.csr.2007.06.008.

References

Anderson, D.M., 1997. Bloom dynamics of toxic *Alexandrium* species in the northeastern United States. Limnology and Oceanography 42 (5 part 2), 1009–1022.

Anderson, D.M., Keafer, B.A., Geyer, W.R., Signell, R.P., Loder, T.C., 2005a. Toxic *Alexandrium* blooms in the Gulf of Maine: the "plume advection hypothesis" revisited. Limnology and Oceanography 50 (1), 328–345.

Anderson, D.M., Keafer, B.A., McGillicuddy, D.J., Mickelson, M.J., Keay, K.E., Libby, P.S., Manning, J.P., Mayo, C.A., Whittaker, D.K., Hickey, J.M., He, R.Y., Lynch, D.R., Smith, K.W., 2005b. Initial observations of the 2005 *Alexandrium fundyense* bloom in southern New England: general patterns and mechanisms. Deep-Sea Research Part II—Topical Studies in Oceanography 52 (19–21), 2856–2876.

Anderson, D.M., Stock, C.A., Keafer, B.A., Nelson, A.B., Thompson, B., McGillicuddy, D.J., Keller, M., Matrai, P.A., Martin, J., 2005c. *Alexandrium fundyense* cyst dynamics in the Gulf of Maine. Deep-Sea Research Part II—Topical Studies in Oceanography 52 (19–21), 2522–2542.

Bauerfeind, E., Elbrachter, M., Steiner, R., Throndsen, J., 1986. Application of Laser Doppler Spectroscopy (LDS) in determining swimming velocities in motile phytoplankton. Marine Biology 93 (3), 323–327.

Bigelow, H.B., 1927. Physical oceanography of the Gulf of Maine. Fisheries Bulletin 40, 511–1027.

Blumberg, A.F., Mellor, G.L., 1987. A description of a three-dimensional coastal ocean circulation model. In: Heaps, N. (Ed.), Three-Dimensional Coastal Ocean Models. American Geophysical Union, pp. 1–16.

Brooks, D.A., 1985. Vernal circulation in the Gulf of Maine. Journal of Geophysical Research 90 (C3), 4687–4705.

Carpenter, E.J., Guillard, R.R.L., 1971. Intraspecific differences in the nitrate half-saturation constants for three species of marine phytoplankton. Ecology 52 (1), 183–185.

Chai, F., Dugdale, R.C., Peng, T.H., Wilkerson, F.P., Barber, R.T., 2002. One-dimensional ecosystem model of the equatorial Pacific upwelling system. Part I: model development and silicon and nitrogen cycle. Deep-Sea Research Part II—Topical Studies in Oceanography 49, 2713–2745.

Denman, K.L., Pena, M.A., 1999. A coupled 1-D biological/physical model of the northeast subarctic Pacific Ocean with iron limitation. Deep Sea Research Part II—Topical Studies in Oceanography 46, 2877–2908.

Droop, M.R., 1983. 25 years of algal growth kinetics, a personal view. Botanica Marina 26 (3), 99–112.

Eppley, R.W., Thomas, W.H., 1969. Comparison of half-saturation "constants" for growth and nitrate uptake of marine phytoplankton. Journal of Phycology 5, 365–369.

Eppley, R.W., Rogers, J.N., McCarthy, J.J., 1969. Half-saturation constants for uptake of nitrate and ammonium by marine phytoplankton. Limnology and Oceanography 14 (6), 912–920.

Etheridge, S.M., Roesler, C.S., 2005. Effects of temperature, irradiance, and salinity on photosynthesis, growth rates, total toxicity, and toxin composition for *Alexandrium fundyense* isolates from the Gulf of Maine and Bay of Fundy. Deep Sea Research Part II—Topical Studies in Oceanography 52 (19–21), 2491–2500.

Flather, R.A., 1976. A tidal model of the north-west European continental shelf. Memoires Societe Royale des Sciences de Liege 6 (10), 141–164.

Fong, D.A., Geyer, W.R., Signell, R.P., 1997. The wind forced response of a buoyant coastal current: observations in the western Gulf of Maine. Journal of Marine Systems 12 (1), 69–81.

Franks, P.J.S., Anderson, D.M., 1992a. Alongshore transport of a toxic phytoplankton bloom in a buoyancy current: *Alexandrium tamarense* in the Gulf of Maine. Marine Biology 112 (1), 153–164.

Franks, P.J.S., Anderson, D.M., 1992b. Toxic phytoplankton blooms in the Gulf of Maine: testing hypotheses of physical control using historical data. Marine Biology 112 (1), 165–174.

Fung, I.Y., Harrison, D.E., Lacis, A.A., 1984. On the variability of the net longwave radiation at the ocean surface. Reviews of Geophysics and Space Physics 22 (2), 177–193.

Garside, C., Garside, J.C., Keller, M.D., Sieracki, M.E., 1996. The formation of a high nutrient–low salinity water in the Gulf of Maine: a nutrient trap? Estuarine, Coastal and Shelf Science 42, 617–628.

Geyer, W.R., Gardner, G.B., Brown, W.S., Irish, J., Butman, B., Loder, T.C., Signell, R.P., 1992. Physical Oceanographic Investigations of Massachusetts and Cape Cod Bays. Woods Hole Oceanographic Institution, Woods Hole.

Geyer, W.R., Signell, R.P., Fong, D.A., Wang, J., Anderson, D.M., Keafer, B.A., 2004. The freshwater transport and dynamics of the western Maine Coastal Current. Continental Shelf Research 24 (12), 1339–1357.

Kamykowski, D., Reed, R.E., Kirkpatrick, G.J., 1992. Comparison of the sinking velocity, swimming velocity, rotation and path characteristics among six marine dinoflagellate species. Marine Biology 113 (2), 319–328.

Keafer, B.A., Churchill, J.H., McGillicuddy, D.J., Anderson, D.M., 2005. Bloom development and transport of toxic *Alexandrium fundyense* populations within a coastal plume in the Gulf of Maine. Deep-Sea Research Part II—Topical Studies in Oceanography 52 (19–21), 2674–2697.

Kelly, J.R., Doering, P.H., 1997. Monitoring and modeling primary production in coastal waters: studies in Massachusetts Bay 1992–1994. Marine Ecology Progress Series 148, 155–168.

Kuhl, M., Jorgensen, B.B., 1994. The light of microbenthic communities: radiance distribution and microscale optics of sandy coastal sediments. Limnology and Oceanography 39 (6), 1368–1398.

Langdon, C., 1987. On the causes of interspecific differences in the growth–irradiance relationships for phytoplankton. Part I. A comparative study of the growth irradiance relationships of three marine phytoplankton species: *Skeletonema costatum, Olithodiscus luteus* and *Gonyaulax tamarensis*. Journal of Plankton Research 9 (3), 459–482.

Large, W.G., Pond, S., 1981. Open ocean momentum flux measurements in moderate to strong winds. Journal of Physical Oceanography 11 (3), 329–336.

Large, W.G., Pond, S., 1982. Sensible and latent heat flux measurements over the ocean. Journal of Physical Oceanography 12 (5), 464–482.

Liebig, J., 1845. On chemical processes in the nutrition of vegetables. In: Playfair, L., Peterson, P.A. (Eds.), Chemistry and its Applications to Agriculture and Physiology.

Lomas, M.W., Glibert, P.M., 2000. Comparison of nitrate uptake, storage, and reduction in marine diatoms and flagellates. Journal of Phycology 36 (5), 903–913.

Luerssen, R.M., Thomas, A.C., Hurst, J.W., 2005. Relationships between satellite-measured thermal features and *Alexandrium*-imposed toxicity in the Gulf of Maine. Deep-Sea Research Part II—Topical Studies in Oceanography 52 (19–21), 2656–2673.

Luettich, R.A., Westerink, J.J., Scheffner, N.W., 1992. ADCIRC: an advanced three-dimensional circulation model for shelves, coasts and estuaries, Report 1: Theory and methodology of ADCIRC-2DDI and ADCIRC-3DL. Technical Report DRP-92-6, Dredging Research Program, Department of the Army, Washington, DC.

Lynch, D.R., Naimie, C.E., 1993. The M2 tide and its residual on the outer banks of the Gulf of Maine. Journal of Physical Oceanography 23 (10), 2222–2253.

Lynch, D.R., Holboke, M.J., Naimie, C.E., 1997. The Maine coastal current: spring climatological circulation. Continental Shelf Research 17 (6), 605–634.

MacIsaac, J.J., Grunseich, G.S., Glover, H.J., Yentsch, C.M., 1979. Light and nutrient limitation in *Gonyaulax excavata*: nitrogen and carbon trace results. In: Toxic Dinoflagellate Blooms: Proceedings of the Second Conference on Toxic Dinoflagellate Blooms. Elsevier/North-Holland, pp. 107–110.

Martorano, C.D., Loder, T.C., 1997. Nutrient dynamics during blooms of *Alexandrium* spp. in the southwestern Gulf of Maine. Masters Thesis, University of New Hampshire, Durham, NH, USA.

McGillicuddy, D.J., Anderson, D.M., Solow, A.R., Townsend, D.W., 2005. Interannual variability of *Alexandrium fundyense* abundance and shellfish toxicity in the Gulf of Maine. Deep-Sea Research Part II—Topical Studies in Oceanography 52 (19–21), 2843–2855.

Naimie, C.E., Loder, J.W., Lynch, D.R., 1994. Seasonal variation in the three-dimensional residual circulation on Georges Bank. Journal of Geophysical Research 99 (C8), 15,967–15,989.

Petrie, B., Yeats, P., 2000. Annual and interannual variability of nutrients and their estimated fluxes in the Scotian Shelf–Gulf of Maine region. Canadian Journal of Fisheries and Aquatic Science 57, 2536–2546.

Platt, T., Jassby, A.D., 1976. The relationship between photosynthesis and light for natural assemblages of coastal marine phytoplankton. Journal of Phycology 12 (4), 421–430.

Prakash, A., 1967. Growth and toxcity of a marine dinoflagellate, *Gonyaulax tamarensis*. Journal of the Fisheries Research Board of Canada 24 (7), 1589–1606.

Shumway, S.E., Sherman-Caswell, S., Hurst, J.W., 1988. Paralytic shellfish poisoning in Maine: monitoring a monster. Journal of Shellfish Research 7 (4), 643–652.

Sommer, U., 1991. A comparison of the Droop and Monod models of nutrient limited growth applied to natural populations of phytoplankton. Functional Ecology 5 (4), 535–544.

Spitz, Y.H., Newberger, P.A., Allen, J.S., 2003. Ecosystem response to upwelling off the Oregon coast: behavior of three nitrogen based models. Journal of Geophysical Research, Oceans 108 (C3), 3062.

Stock, C.A., McGillicuddy, D.J., Solow, A.R., Anderson, D.M., 2005. Evaluating hypotheses for the initiation and development of *Alexandrium fundyense* blooms in the western Gulf of Maine using a coupled physical–biological model. Deep-Sea Research Part II—Topical Studies in Oceanography 52 (19–21), 2715–2744.

Townsend, D.W., Cammen, L.M., 1988. Potential importance of the timing of spring plankton blooms to recruitment of juvenile demersal fishes. Biological Oceanography 5, 215–229.

Townsend, D.W., Pettigrew, N.R., Thomas, A.C., 2001. Offshore blooms of the red tide dinoflagellate *Alexandrium* sp., in the Gulf of Maine. Continental Shelf Research 21 (4), 347–369.

Watras, C.J., Chisholm, S.W., Anderson, D.M., 1982. Regulation of growth in an estuarine clone of *Gonyaulax tamarensis* Lebour: salinity-dependent temperature responses. Journal of Experimental Marine Biology and Ecology 62 (1), 25–37.

Zielinsky, G.A., Keim, B.D., 2003. New England Weather and Climate. University Press of New England, Lebanon, NH.